THE ASTROPHYSICAL JOURNAL, 484:900–919, 1997 August 1

THE VECTOR MAGNETIC FIELDS AND THERMODYNAMICS OF SUNSPOT LIGHT BRIDGES: THE CASE FOR FIELD-FREE DISRUPTIONS IN SUNSPOTS

K. D. LEKA[1]
High Altitude Observatory and Advanced Study Program, National Center for Atmospheric Research, Boulder, CO 80303
Received 1996 October 8; accepted 1997 February 28

ABSTRACT

We present observations with the Advanced Stokes Polarimeter of 11 light bridges in sunspots of various ages and sizes, all very close to disk center. Full vector spectropolarimetry and a nonlinear least-squares inversion algorithm allows us to determine not only the vector magnetic field in the bridges and host sunspots but also thermodynamic parameters such as continuum brightness, Doppler shifts, Doppler widths, opacity ratio, and the source function parameters. We can also separate the magnetic and nonmagnetic components of the spectral signal within each resolution element.

We find that there is a disruption of the magnetic fields in light bridges, relative both to neighboring umbrae and to normal, undisturbed penumbrae. This change takes the form of lower intrinsic field strength and sparser, more horizontal fields in the bridges relative to umbrae. The magnetic fields in the bridges remain more vertically oriented, however, than those in undisturbed penumbra. There are systematic upflows observed in the bridge plasma relative to the neighboring umbrae, and the evidence points toward a component that is heated and departs from radiative equilibrium.

In four cases, we follow a light bridge over several days and find that as the bridges age, they grow wider and brighter, the fields weaken and become sparser, and the heating increases. We also find some evidence that the magnetic field begins to reorganize itself to accommodate the (now) two azimuth centers *before there are strong signals of a light bridge in the thermodynamic parameters.*

This paper presents the first systematic look at sunspot light bridges with full vector polarimetry and thermodynamic determination. The results show that there is an intrusion of field-free, possibly convective material into an otherwise stable, magnetic sunspot. The departure from stability is seen in the magnetic field orientation *prior* to its appearance in continuum intensity, and the effects of this disruption are evident beyond the immediate umbral intrusion. The results do *not* unambiguously determine the physical mechanism that makes sunspots disappear. However, it strongly points toward a ropelike magnetic structure through which convection may penetrate when the magnetic fibrils separate or around which field-free plasma may flow. The appearance of field-free heated material is likely an effect, not the cause, of the sunspot light bridges.

Subject headings: polarization — Sun: magnetic fields — sunspots

1. INTRODUCTION

Considering how well observed sunspots are, it is often surprising how poorly some of their structures and evolutionary processes are understood. Sunspot dissolution and disappearance is a phenomena with less immediate impact than, say, flux emergence or the evolution associated with complicated, flare-productive active regions. How a sunspot "dies" is poorly understood even at the most basic, cartoon level. The question of whether a sunspot fragments, submerges, is expelled, or diffuses in place is unanswered. Yet in terms of some long-standing questions in solar physics (such as the overall solar magnetic flux budget or how the polar field is generated), the question of a sunspot's fate is in fact *more* important than how it arrived.

One of the early signatures of imminent sunspot breakup is the formation of a light bridge: an intrusion, or lane of bright material that cuts across the umbra of a sunspot (Bray & Loughhead 1964). Light bridges "show a great diversity in shape, size, and brightness" (Bray & Loughhead 1964, p. 89), so of course historically their definitions and categorizations have been numerous and diverse. The morphological classifications based on their intensity have essentially been "photospheric," "penumbral," and "umbral." The first class can refer to a wide separation between sunspot umbrae that is clearly inhabited by photospheric, granular-looking material. The latter two categories usually refer to bridges where penumbral-appearing material cuts across the umbra, the "penumbral" bridges being larger than "umbral" bridges (Muller 1979; Bumba & Suda 1983; Sobotka 1989; Sobotka, Bonet, & Vázquez 1993). The classifications get confusing when subclasses based on bridge width in addition to brightness are added (Sobotka et al. 1993; Sobotka, Bonet, & Vázquez 1994) and when the classes refer to umbrae of the same (or opposite) magnetic polarity (Bumba & Hejna 1980; Ogir, Parkinenko, & Stoyanova 1985; Zirin & Wang 1990; Sobotka et al. 1994). We make no attempt to classify the bridges studied in this paper a priori, except that none fall into those categories in which the material observed is clearly photospheric in nature (i.e., similar in brightness to quiet photosphere, with easily discernible granulation patterns). The bridges studied herein have a range of widths, ages, and intensities and undoubtedly span more than one morphological classification boundary. To wit, we simply empha-

[1] The National Center for Atmospheric Research is sponsored by the National Science Foundation.

size that the sunspot light bridges referred to hereafter are those that (1) split umbrae of like polarity, (2) are generally narrow (≤ 10 Mm across), and (3) are dominantly of penumbral, not photospheric, intensity

Based on white-light morphology alone, light bridges may be the result of the coalescence of pores as a sunspot grows, the bridges' contrast gradually diminishing until a stable sunspot is formed (Bumba & Suda 1983; Garcia de la Rosa 1987; Zirin & Wang 1990). From snapshot morphology alone, it is almost impossible to tell a bridge's history, i.e., whether the presence of a bridge signals sunspot formation or "de-formation." Can those bridges associated with sunspot decline be differentiated a priori from those present during pore coalescence?

Previous studies of light bridges have found that their magnetic fields are generally weaker and more horizontal than in the neighboring umbra (Beckers & Schröter 1969; Lites et al. 1991; Rüedi, Solanki, & Livingston 1995a, 1995b). So far, this is essentially the only systematic finding. Redshifts (Rüedi et al. 1995b), blueshifts (Beckers & Schröter 1969), and "noshifts" (Rüedi et al. 1995b) have been found in light bridges relative to the nearby umbrae. Intensity fine structure that may resemble photospheric granulation (Vázquez 1973; Sobotka et al. 1994; Ogir, Parkinenko, & Stoyanova 1985), penumbral dark filaments and bright grains (Sobotka et al. 1993, 1994), or both (Muller 1979; A. Tritschler 1996, private communication) are found in bridges. Semiempirical models of light bridges indicate a lower temperature, i.e., the bridge regions are darker, than the mean penumbra for a moderate range in optical depth around $\tau = 1.0$ (Sobotka 1989).

One intriguing aspect about light bridges is that whatever magnetic reconfiguration occurs during their formation, it is accompanied by short-lived chromospheric Hα brightenings (Bumba, Suda, & Ishkov 1981) with counterparts in the corona (Shimizu 1996). Since bridges form within regions of like polarity with no reported observations of intrusions of opposite polarity fields, the standard picture of reconnection between opposite polarity regions (as associated with flares) is difficult to apply to the bridge magnetic topology where these brightenings occur.

The major weakness of prior studies has been small number statistics and/or a lack of vector magnetic field data, as commented on in Lites et al. (1991) and Rüedi et al. (1995b). The studies cited so far for the most part have drawn upon white-light photographs and longitudinal magnetograph observations, with occasional spectroscopic observations that sampled a few positions across a light bridge.

We present here a study of numerous light bridges with the Advanced Stokes Polarimeter, with which spatial maps across a sunspot with full spectral and polarimetric coverage are made. In § 2, we present the observations, some details of the inversion procedure, and the interpretation of its output. In § 3, we discuss the physical interpretation of the inversion procedure output in order to set the context for the presentation of the bridge results. In § 4, we begin the analysis by systematically comparing the light bridges both with their neighboring umbrae and with undisturbed areas in the sunspots (i.e., away from the light bridge), without regard to evolutionary history, age, or morphological detail. The overall picture of the physical structure of light bridges is then presented. In § 5, the results from § 4 are used to examine the systematics (or lack thereof) in the results, in the context of the sunspots' histories and evolution. These approaches lead to a discussion of the physical nature of the light bridge formation process.

2. OBSERVATIONS

All observational data used in this paper were gathered with the Advanced Stokes Polarimeter (ASP) at the National Solar Observatories/ Sacramento Peak, New Mexico. The ASP data consist of fully resolved spectra covering 2.5 Å around two Zeeman-sensitive Fe I lines ($\lambda\lambda$6301.5, 6302.5) at 12.6 mÅ dispersion, and 230 pixels (0.″37) in the spatial dimension. The spectrograph slit is stepped across a region of interest on the solar disk, with step size chosen by the observer. All four Stokes parameters (I, Q, U, V) are recorded at each wavelength point on two cameras; the images from these two cameras are merged to produce data hypercubes containing x, y, λ, I, Q, U, V information. The details of the ASP optical layout, performance, and calibration can be found respectively in Elmore et al. (1992), Lites (1996), and Skumanich et al. (1997). From these spectrally, spatially, and polarization-state sampled data, we perform an inversion using the nonlinear least-squares analysis described in Skumanich & Lites (1987). The HAO inversion code independently fits the Stokes profiles with two contribution functions, one from a magnetic modeled atmosphere and one from a nonmagnetic component discussed in detail below. It assumes a Milne-Eddington atmosphere and a source function linear with optical depth $S_\nu(\tau) = fB_0 + fB_1\mu\tau_c$, where B_0, B_1 are magnitudes of the constant and linear terms, τ_c is the continuum optical depth along the line of sight, f is a magnetic filling factor and $\mu = \cos(\theta)$ is the viewing angle. The inversion returns magnetic field strength ($\boldsymbol{B}$), inclination and azimuthal angles (ψ, ζ), an effective nonmagnetic fraction (α'), the constant and linear terms of the source function (fB_0, $fB_1\,\mu$), the line-to-continuum opacity ratio (η_0), the Doppler width ($\Delta\lambda_D$), and the line center positions for the magnetic and nonmagnetic components (λ_{mag}, λ_{nmag}).

The inversion procedure from spectral Stokes profiles to magnetic and thermodynamic parameters can result in nonunique solutions owing to noise, improper weighting of the profiles, etc. In general, the vector magnetic field parameters are much better known than the thermodynamic results, among which there can be some interplay in the results (Lites & Skumanich 1990). However, in the sunspots analyzed, there are no differences in the errors for the fits between bridge areas and nonbridge areas. The line profiles are not inherently different for the most part (given the χ^2 restrictions discussed below), and the fits were all confirmed visually. Hence, we believe that any trends we present in the magnetic and thermodynamic parameters will be evidence of true physical differences between the light bridge and the normal sunspot structure.

Data from eight observing runs were used, covering 11 different light bridges in nine sunspots. For most bridges, multiple observations were available on the same day; for four bridges, data were also available a day or two later. In Table 1, we list the observational parameters and NOAA Active Region numbers of all data which were analyzed (Solar Geophysical Data 1992–1996), and in Figure 1, we show the sunspot continuum images. Usually only the data set with the best overall seeing and that was closest to disk center is represented in the subsequent tables and figures. The other data, when available, were used to confirm results

TABLE 1

LIGHT BRIDGES AND THEIR SUNSPOTS

Bridge	Active Region (NOAA)	Date	Time (UT)	μ	Seeing (arcsec)
1a	7108	1992 Mar 20	15:20	0.84	1
			15:51		1.5
1b	7108	1992 Mar 22	14:54	0.96	2
2	7192	1992 Jun 11	16:05	0.92	1
			13:56		1.5
3	7194	1992 Jun 14	15:08	0.95	1.5
4	7194	1992 Jun 16	15:52	0.95	1.
5	7465	1993 Apr 4	15:36	1.0	≤ 1
			14:17		1
			14:42		≤ 1
			16:54		2
6a	7548	1993 Jul 23	14:46	0.94	≤ 1
6b	7548	1993 Jul 24	15:10	0.88	≤ 1
			14:00		1.5
			14:25		1–1.5
			15:02		1
			17:25		2
			17:41		1.5–2
7a	7597	1993 Oct 13	14:57	0.84	≤ 1
			15:37		1
7b	7597	1993 Oct 14	14:29	0.88	1
8, 9.....	7722	1994 May 17	15:23	0.98	≤ 1
			14:00		1.5
			14:25		1–1.5
			15:02		1
			16:07		≤ 1
			17:25		2
			17:41		1.5–2
10	7952	1996 Mar 14	17:53	0.99	1
11a.....	7962	1996 May 12	16:12	1.0	≤ 1
			15:20	0.99	1
			16:00	1.0	≤ 1
11b.....	7962	1996 May 13	14:22	1.0	≤ 1
			14:32	0.99	1
			14:45		1
			15:37		1
			16:15		1.5

presented here and are listed after the primary data set. For example, Bridge 6b was observed for many hours, with relatively good seeing; the data set at 15:10 UT was the primary data set from which the results shown here were derived, and the remainder for Bridge 6b were used as confirmation. The study of the temporal evolution of the bridges is restricted to daily changes for this study, e.g., the observations of the same bridge on 1992 March 20 and 22, labeled Bridge 1a and 1b. Hourly changes in the magnetic and thermodynamic parameters are generally smaller and are not considered here. Table 2 gives some of the basic morphological parameters of the bridges and their host sunspots, such as the host sunspot's age (Solar Geophysical Data 1992–1996), magnetic polarity, and the light bridge widths.

The requirements for data to be included in this study were fairly stringent. The light bridges had to be fairly simple and distinct, and a large portion of the host sunspot had to be "undisturbed" for comparison. Seeing had to be nominally 1″, and $\mu = \cos(\theta) \geq 0.85$. This last requirement is for two reasons. First, it has been reported that the boundary between a bridge and the neighboring umbra is narrow, of order 1″ (Rüedi et al. 1995b). Observations need to be close to disk center to avoid confusion that arises if the line-of-sight radiation propagation vector crosses strongly varying atmospheres within the height of formation. Second, at $\mu \leq 0.85$, the V profiles from midpenumbra outward consistently show evidence of reversed polarity within the pixels owing to the coupling of high field inclination with a high viewing angle in addition to velocity gradients and the like (see, e.g., Skumanich & Lites 1991; Bünte, Steiner, & Solanki 1991). This is confusion that we wish to avoid. Although the HAO inversion code has recently been upgraded to three components (two magnetic in addition to a nonmagnetic component), the most

TABLE 2

LIGHT BRIDGES AND THEIR SUNSPOTS: BASIC PROPERTIES

Bridge	Magnetic Polarity	AR Age (days)	Spot Area (Mm^2)	⟨Width⟩ (Mm)	Width Range (Mm)
1a	−	31+ (7067)	722	3.0	0–5
1b	−	33+	528	4.6	—
2	−	8+	459	5.8	0–10
3	+	25 (7176)	573	3.2	2.3–4.6
4	+	26 (7176)	487	3.7	0–9.5
5	+	8+ (7400)[a]	906	3.0	0–6.5
6a	+	7+	759	2.4	0–3.8
6b	+	8+	751	3.0	0–7.4
7a	−	5+	463	1.8	—
7b	−	6+	333	2.2	1.4–3.5
8	−	33+ (7701)[b]	1357	3.8	—
9	−	33+ (7701)[b]	1357	5.6	2.4–7.0
10	+	3	217	3.9	0–5.3
11a.....	+	22 (7958)	240	2.1	1.4–4.6
11b.....	+	23	190	3.6	—

NOTE.—In parentheses, the AR identified from the previous rotation. The "+" indicates that the active region was formed prior to arriving at the east limb but could not be identified with an active region in the previous rotation, i.e., "8+" indicates an active region between 8 and 23 days old. The ages of the individual spots are more difficult to determine, except that in all cases but Bridge 10, the sunspots themselves appeared, formed and stable, at the east limb. A "—" in the width range indicates an almost constant width across the bridge.

[a] Bridge 5 is part of the active longitude that began with AR 7400, 1993 Jan 12, and returned as 7420, 7440 and then 7465. The individual spot used here, however, was most likely not 83 days old, but rather between 8 and 23 days old.

[b] AR 7722's identification with AR 7701 might also be AR 7708, which would make it 21 days old (instead of 33+).

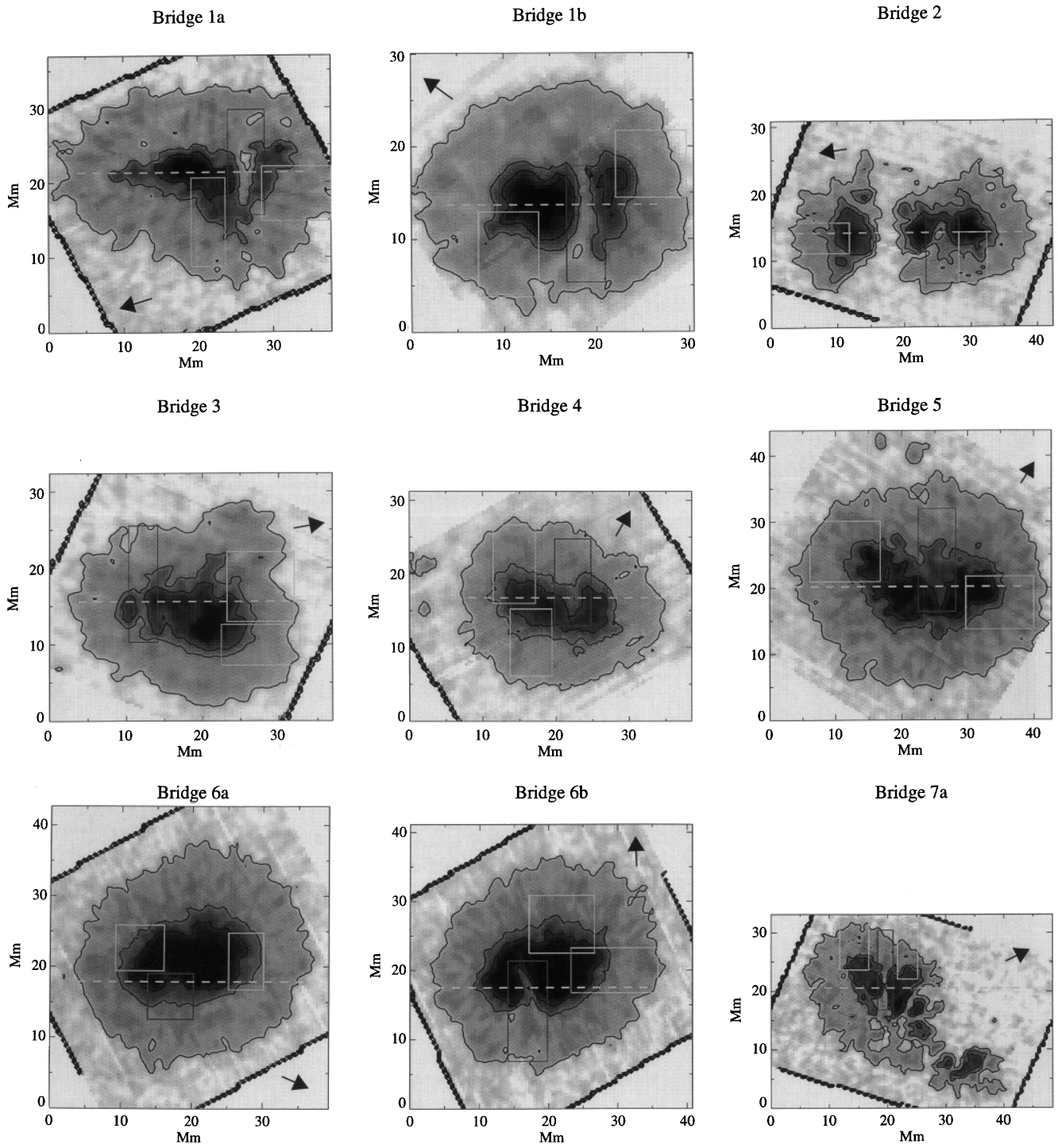

FIG. 1.—Gray-scale continuum images of the sunspots studied in this paper, and their designations as per Table 1, with the heliographic scale shown in megameters. Boxes drawn in show the Regions of Interest (ROI) for the light bridge (*dark gray box*) and for undisturbed areas (*light gray boxes*). The horizontal dashed line indicates where our artificial spectrograph slit was placed. For all sunspots, north and east are at random orientations, since the data were rotated such that the boxes and "slit" position could be positioned easily. The direction to disk center is shown, and contours indicate the umbral, transition zone, and penumbral areas on each sunspot (see Fig. 2).

straightforward interpretation comes from the standard two-component fitting. Thus, we restrict ourselves to sunspots and light bridges that are close to disk center and further restrict the studied sunspot areas to those that had $\chi^2(V)/V^2 \leq 0.1$.

An objective, non–morphology-based definition of a light bridge is not available in the literature. Indeed, even an objective manner to define the photospheric/penumbral/umbral boundaries could not be found in the context of sunspot studies (although it has been mentioned in the context of solar irradiance studies; e.g., Steinegger et al. 1996 and references therein). Since the objective of this study is to determine the physical state of the light bridge, it behooves us *not* to use any ad hoc boundaries for the light bridges and *not* to use any morphological classification or categorization scheme before examining the data. Instead,

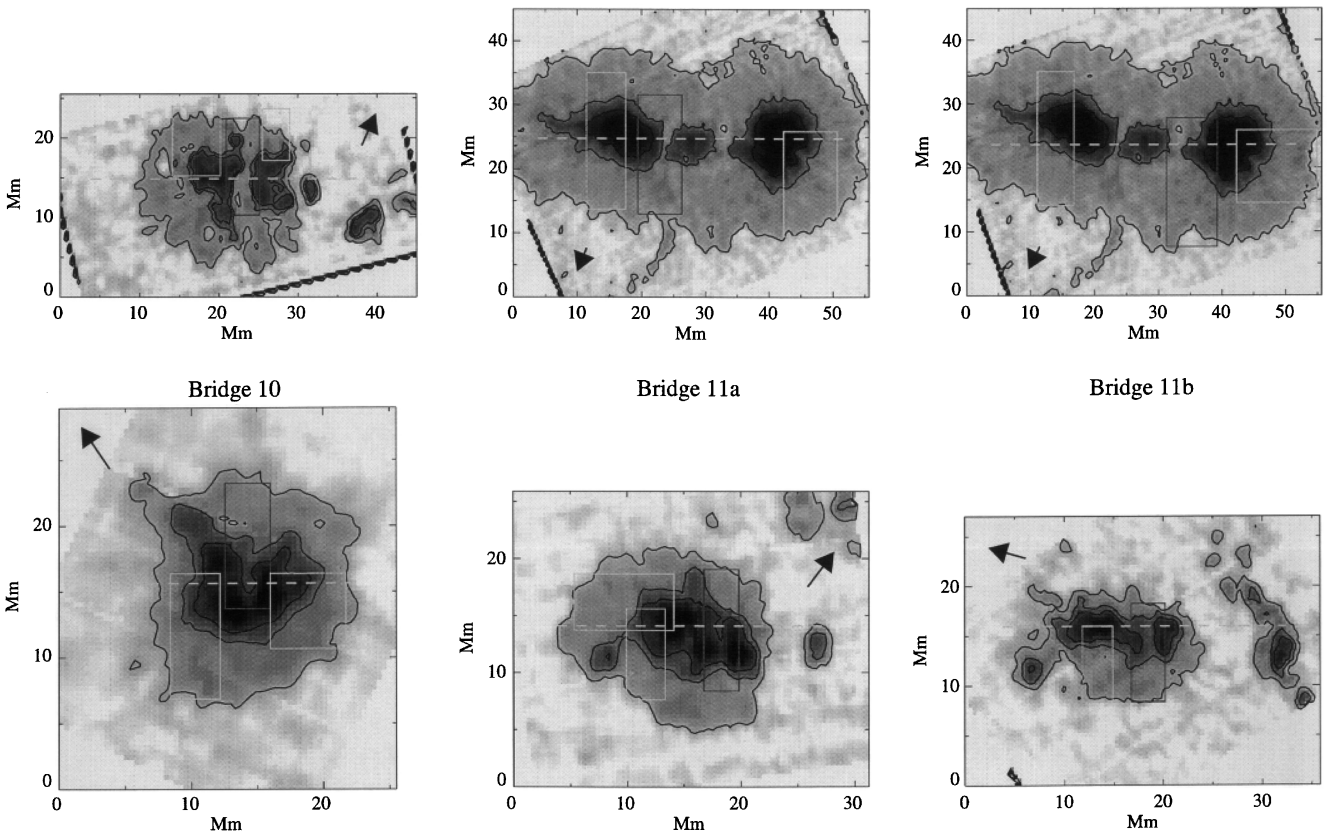

FIG. 1—*Continued*

we utilize large sampling regions that encompass the classically identifiable light bridge, along with surrounding umbra and penumbra. We are explicitly stating with this approach, that we do not know what is physically responsible for, or affected by, the formation of the bridge. Hence, we do not draw any boundaries to define the extent of the light bridge a priori.

We must, however, adopt some definition of umbra and penumbra to facilitate interbridge comparisons. To do so, we used the following observation: a histogram of the continuum intensity consistently showed four distributions (Fig. 2; see also Steinegger et al. 1996, Fig. 2). At the brightest intensities is the peak associated with quiet Sun; the most probable value for this peak is taken as the mean quiet Sun intensity [I_c(qs)], used for normalization through the rest of the paper. At slightly smaller intensity values, there is a second peak whose distribution defines the proper penumbra. The minimum between these two, or where the derivative of the distribution crosses zero, is taken as the intensity that defines the outer penumbral boundary [0.92 I_c(qs) in the example shown]. At the lowest continuum intensities, there is a small peaked distribution; this represents the dark umbral cores. At the upper bound of this distribution, the derivative again crosses zero, defining an intensity level that bounds the dark umbra [0.37 I_c(qs) in this example]. Between the dark umbra and the penumbra is a range of intensities where the frequency is almost constant. This defines a region between the umbra and penumbra. Where this flat distribution ends and the penumbra begins is the end of what we deem the transition zone [0.37–0.70 I_c(qs)]. Its width (both physically and in terms of the range of intensities in the distribution) varies slightly. These four distributions in the intensity histograms were always distinguishable, and the resulting intensity contours are given in Figure 2 for the example and are also reflected in Figure 1. We find this method to be reasonably insensitive to the effects of bad seeing, and only the width of the transition zone is in the least affected. The same distribution is visible and the same results are obtained when the seeing is artificially degraded by rebinning the data by a factor of 5.

The orientation of each bridge relative to solar north was arbitrary. To ease the analysis process, the data for each bridge (magnetic field map, velocity map, etc.) was rotated by an arbitrary angle such that the light bridge was oriented roughly along the $\hat{y}$ axis. The bridges as shown in Figure 1 have been rotated in this fashion. We indicate the direction to disk center for reference.

As stated above, we wished to investigate the physics of the bridges with few restrictions. Hence we defined a rectangular region of interest (an "ROI") that encompassed the bridge and surrounding umbra and penumbra. These ROIs are shown in Figure 1. In addition, we selected additional ROIs for comparison around undisturbed, nonbridge areas of penumbra and umbra. These are also indicated in Figure 1. Between each ROI, the number of umbral, transition zone, and penumbral points were equalized to about

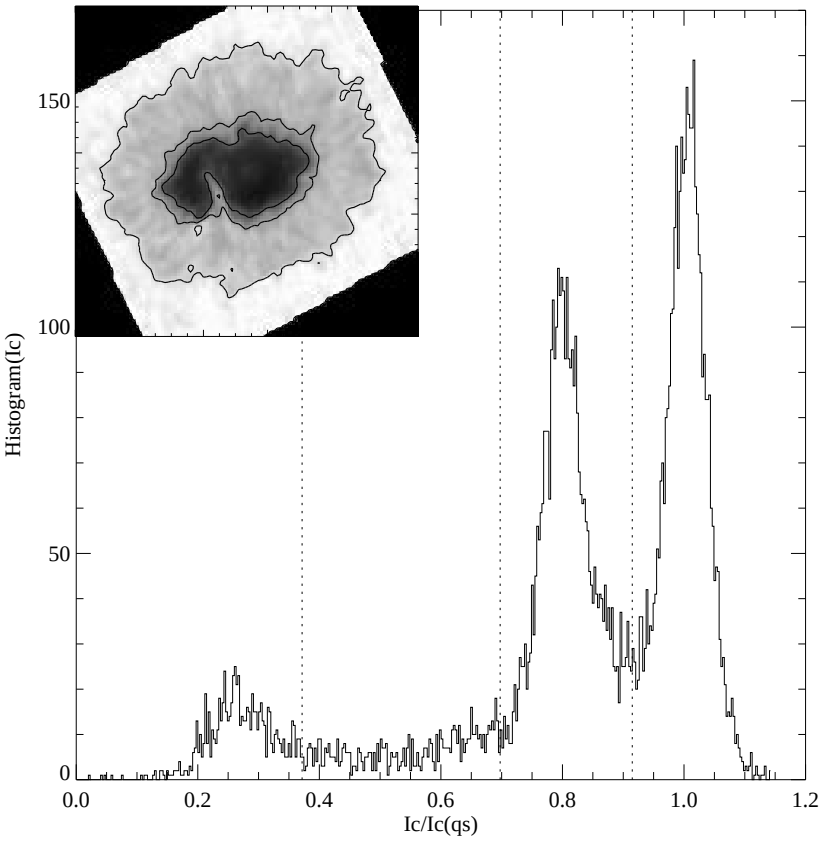

FIG. 2.—Determination of region-defining isophotes using Bridge 6b as an example. Histogram of the continuum intensity, I_c, is shown for the sunspot. The light levels which were chosen to define the umbral core, the umbral-penumbral transition zone, and the outer penumbral boundary are indicated by vertical dashed lines. *Inset*: continuum image of Bridge 6b showing the three contours.

10%, so that the effects of unequal statistics were minimized. As mentioned above, we also excluded data points with a $\chi^2(S_j)/S_j^2 \geq 0.1$ for the fits to $S_j = [Q, U, V]$.

We also wished to compare with previous studies that positioned a spectrograph slit across a sunspot. To do this, we chose an artificial "slit position," or row, that traversed the bridge at its approximate center and also included neighboring umbral region(s). Along this "slit," or row, we can plot magnetic and thermodynamic parameters, similar to the approach taken by earlier spectroscopic investigations of these features (Sobotka 1989; Rüedi et al. 1995b). These artificial slit positions are also indicated in Figure 1.

3. INTERPRETING THE DATA

3.1. *The Magnetic Vector*

Even though the intrinsic magnetic field strength $\boldsymbol{B}$ and the two directional angles ψ and ζ are returned by the inversion code, the transverse field component's direction is unsigned. To resolve this 180° ambiguity, two methods were used: the interactive "AZAM" procedure (written in the Interactive Data Language by P. Seagraves; Lites et al. 1995) essentially uses a radiant point chosen close to the sunspot's center along with continuity arguments to resolve the ambiguity. This is supplemented, when required, by selecting the azimuth closest to that of a potential field calculated using the line-of-sight field as a boundary condition. While this algorithm may be problematic for highly sheared fields, or sunspots viewed close to the limb, in general the light bridges and their host sunspots studied here had fairly simple magnetic structures and were close to disk center. The second method is an iterative technique (Canfield et al. 1993; Leka 1995) that minimizes the angle difference between neighboring vectors and minimizes either the vertical current or the divergence of the field according to field strength criteria. (The latter results are also identical, for these simple spots, to that from the "simulated annealing" algorithm; Metcalf 1994.) The ambiguity-resolved magnetic vector $\boldsymbol{B}$ and other output data (e.g., line center position, etc.) were projected then to a local tangent plane, i.e., to an apparent $\mu = 1.0$ viewing angle, and interpolated on to a grid with approximately 0.″5 square pixels. Henceforth, all vector angles (i.e., γ, ϕ) are in the heliographic frame, i.e., as if one were looking down upon the sunspot.

3.2. *Magnetic Filling Factor*

The "scattered" light fraction, α, is specifically the fraction of a pixel filled with an unmodeled nonmagnetic signal. That is, the total intensity, I_λ, is a combination of the calculated model signal $I_\lambda^{\rm mod}$ and light scattered into the resolution element, presumably from a nonmagnetic photosphere. In general, we may consider the model to be given by

$$I_\lambda^{\rm obs} = I_\lambda^{\rm mod} + \alpha I_\lambda^{\rm scat} ,$$

where

$$I_\lambda^{\rm mod} = f I_\lambda^{\rm mag} + (1-f) I_\lambda^{\rm nmag} ,$$

with $I_\lambda^{\rm mag} = \mathscr{F}(|\boldsymbol{B}|, \psi, \zeta, \eta_0, B_0, B_1, \text{etc.})$, and $(1-f)$ is the fraction of the resolution element filled with a field-free

model atmosphere $I_\lambda^{\rm nmag}$. The $I_\lambda^{\rm scat}$ line profile is constructed as an average over pixels that have a polarization fraction below an arbitrary threshold, typically 0.4%. Since the HAO inversion procedure does not differentiate $I_\lambda^{\rm scat}$ from $I_\lambda^{\rm nmag}$ in terms of the model parameters, what the code truly returns[2] is a value α', i.e.,

$$I_\lambda^{\rm obs} = fI_\lambda^{\rm mag} + (1-f)I_\lambda^{\rm nmag} + \alpha I_\lambda^{\rm scat}$$
$$= fI_\lambda^{\rm mag} + \alpha' I_\lambda^{\rm scat} ,$$

where

$$\alpha' = (1-f)(I_\lambda^{\rm nmag}/I_\lambda^{\rm scat}) + \alpha .$$

Note that $fI_\lambda^{\rm mag} = I_\lambda^{\rm mag}(fB_0, fB_1)$ where f is unknown. Interested readers are referred to Skumanich, Grossmann-Doerth, & Lites (1992) for a full discussion. Unless otherwise stated, the plots, results, and discussion refer to α'.

3.3. *Doppler Shifts of $I_\lambda^{\rm mag}$ and $I_\lambda^{\rm nmag}$*

The observed solar photosphere is not stationary, and the signals from the vertical component of any bulk flow will be detected as a Doppler shift. The results from the inversion code allow us to determine separately the line center position of $I_\lambda^{\rm mag}$ and $I_\lambda^{\rm nmag}$ ($\lambda_0^{\rm mag}$ and $\lambda_0^{\rm nmag}$, respectively), although the latter has significantly larger uncertainty. Throughout (unless noted), we use the umbral $\lambda_0^{\rm mag}$ as the reference wavelength (using either the mean of multiple points or the value at one point, depending upon application). Some of the observed Doppler shifts are undoubtedly influenced by "noise" in the form of acoustic oscillations and Evershed flows. However, we note the following points. First, the Evershed effect is most prominent in the outer, brightest penumbral regions; in the analysis of the light bridges, we incorporate data from all intensity ranges. None of the results for the bridges relies solely on points in the brightest intensity bin or on farthest distances from the umbra. Second, while we cannot filter for oscillation signals owing to the stepping-slit nature of the instrument, we note that velocity signals from magnetized plage and sunspot penumbrae have an rms less than 0.3 km s^{-1} (Title et al. 1992). Since our velocity measurements average over space and/or time, any observed trends are the average over the oscillation signals. Additionally, the oscillation periods are generally short compared to the time to acquire a magnetic map. Hence, oscillation signals may increase the width of the distributions of observed Doppler flows but should not affect their median values. Third, we note that the results for the bridges presented below are not a function of $\mu = \cos(\theta)$ or of whether the umbral reference is limbward or diskward of the bridge or normal areas. Fourth, for spots with multiple observations on the same day, we find that the results are statistically the same, to the limit of the uncertainties.

3.4. *Utilizing the Source Function*

3.4.1. *The Ratio B_1/B_0*

The inversion code's use of a linear source function with continuum optical path, $S_\nu(\tau) = fB_0 + fB_1\mu\tau_c$ (Skumanich & Lites 1987) implies that the ratio fB_1/fB_0 removes the fill factor and normalizes the two constants, which allows a direct interpretation of the source function's gradient. That is, this ratio holds implications for the relation between the radiation field and the emergent mean intensity as a function of optical depth. We can use this ratio to compare the state of atmosphere with an atmosphere known to be in approximate radiative equilibrium, i.e., the sunspot umbrae (where the strong magnetic fields suppress convection). We find that for the sunspot umbrae in these data, the average ratio $\overline{B_1/B_0} = 2.1 \pm 0.5$, similar to what is found with other ASP observations (e.g., Skumanich, Lites & Martínez Pillet 1994). Hence, if B_1/B_0 becomes significantly larger than 2, the source function is steeper with depth, which implies that the radiation field is heating the region in excess of what is required for radiative equilibrium (see the discussion in Kourganoff 1952, § 13, and Mihalas 1978, § 2).

3.4.2. *Determining Temperature from the Source Function*

The inversion code returns the source function as a fitted parameter of the nonlinear least-squares procedure. Since for these sunspots, $\mu \approx 1$, we can use the Eddington-Barbier relation, which states that the "emergent intensity is characteristic of the value of the source function at about optical depth unity along the line of sight" (Mihalas 1978). We first compute the fitted continuum intensity for the magnetic component, $I_c^{\rm mag} = fB_0 + fB_1\mu$ and correct it for magnetic filling fraction f by assuming $f = 1. - \alpha'$. We then normalize the ASP's intensity units to the intensity at a nearby continuum wavelength (3.11×10^{14} ergs cm^{-2} s^{-1} sr^{-1} cm^{-1} at $\lambda = 6306.0$ Å; Labs & Neckel 1968). This emergent intensity is then equated to the Planck function, B_ν, and the relevant temperature for $\tau = 1$, T_{B_ν} is calculated. The temperatures fall within the range of recent umbral and penumbral models, $3500 \leq T_{B_\nu} \leq 5500$ K (Collados et al. 1994; del Toro Iniesta, Tarbell, & Ruiz Cobo 1994). The resulting temperatures may not be accurate on an absolute scale; however, constructing a detailed sunspot model is not the goal. This analysis enables us at least to make comparisons between structures within a given ASP data set.

3.5. *Doppler Width $\Delta\lambda_{\rm D}$*

The HAO inversion code returns a value assigned to the Doppler width, $\Delta\lambda_{\rm D}$. This is a measure of the effective line width and includes the true Doppler width of the line, along with unresolved velocity effects such as microturbulence. It is limited in the inversion by theoretical temperature bounds to lie between 20 and 60 mÅ. The implied temperature $T_{\Delta\lambda_{\rm D}}$ in the transition zones and umbrae in all sunspot data fell between $3061 \leq T_{\Delta\lambda_{\rm D}} \leq 4500$ K, but up to $\approx$15,000 K within penumbral boundary.

We can quantify the microturbulence, however, since we have the independent measure of the temperature T_{B_ν} described above. We can then estimate the microturbulence velocity, ξ, by

$$\xi = \left[\frac{2k}{m_{\rm Fe}}\left(T_{\Delta\lambda_{\rm D}} - T_{B_\nu}\right)\right]^{1/2} . \quad (6)$$

The implied microturbulence velocity ξ distributions always peaked $\leq$1.0 km s^{-1} (with $\approx$0.3 km s^{-1} width). This is higher than the $\approx$0.2 km s^{-1} microturbulence velocity from recent sunspot umbral (Collados et al. 1994; the "cool" model) and penumbral (del Toro Iniesta et al. 1994)

[2] Those familiar with the HAO inversion code will note that α' is actually referred to as α within the code and its outputs. One reason for this notation is to distinguish this effective scattered light fraction from the force-free parameter used later.

models. However, it is consistent with the values inferred if one simply compares $T_{\Delta\lambda_D}$ to the umbral and penumbral temperatures derived in these two models. That is, $T_{\Delta\lambda_D} - T_{\text{models}}$ implies $0.2 \leq \xi \leq 0.5$ km s^{-1}.

The variation within an ASP data set of $\Delta\lambda_D$ was larger than the variation in T_{B_ν}. The former is likely dominated by ξ and the (unresolvable) physics within it. That is, ξ varies too widely to be simply subtracted from $\Delta\lambda_D$ in order to determine a reliable $T_{\Delta\lambda_D}$. Instead, we take the Doppler width as a measure of unresolved velocity distributions, relying upon T_{B_ν} for temperature analyses.

3.6. *Line Strength* η_0

The parameter η_0 returned by the HAO inversion code is the line-to-continuum opacity ratio and contains information about the state of the atmosphere in the line-forming region. A smaller value of η_0 indicates a depopulation of the lower energy state, most likely due to enhanced ionization (e.g., in the quiet Sun, where empirically $\eta_0 \approx 10$; see Skumanich et al. 1994). Conversely, if η_0 is larger, it implies that there are more absorbers available to the incident radiation field where the $\lambda\lambda$6301.5, 6302.5 lines are formed, i.e., it is in a cooler, less ionized state. Hence, a change in η_0 between structures gives us information about the heating of the atmosphere in those structures.

4. RESULTS

4.1. *Morphology of Bridges*

In Figure 1, the bridges studied here are shown in continuum intensity images and reflect the conventional wisdom of the wide morphological variety that bridges can have. As varied as they are in these images, they are all intrusions of essentially penumbral-brightness material into the umbra, with like magnetic polarity on either side of the bridge. The sizes of the host sunspots (listed in Table 2 as the area within the outer penumbral brightness level) vary widely. The average width of the bridges varies, although because we limit ourselves to the penumbral-brightness bridges that are still clearly associated with one umbral system, the average widths stay fairly small, under 10 Mm. This average width can be a difficult number to assign, since we are also considering what might be termed "intrusions" in addition to bridges that fully split the umbrae. Again we are not classifying the bridges a priori on the basis of white-light morphology, save that we do not consider the widest bridges comprised of material essentially indistinguishable from normal photosphere. We do not exclude bridges on the basis of small width or incomplete umbral separation. In Table 2, the right-hand column, however, we give the range of widths within the bridge area between umbrae, and unsplit umbrae are indicated there.

4.2. *Light Bridges versus Umbrae*

We compare the bridge regions and neighboring umbra by simulating how one would observe them with a spectrograph slit positioned across the bridge. In Figure 1, we present two examples, Bridges 8 and 10. Nine parameters are considered, three magnetic and six thermodynamic. The magnetic parameters are the intrinsic field strength ($\boldsymbol{B}$) and its deviation from the absolute local vertical ($\Delta\gamma = \gamma$ for $\gamma \leq 90$, $\Delta\gamma = 180 - \gamma$ for $\gamma \geq 90$), and the nonmagnetic fraction (α'). The thermodynamic parameters are the continuum intensity (I_c) relative to the average quiet Sun continuum intensity [I_c(qs)]; the Doppler shift ($\Delta\lambda_0^{\text{mag}}$) of the magnetic component I_λ^{mag} (km s^{-1} relative to the nearby umbra); the Doppler shift ($\Delta\lambda_0^{\text{nmag}}$) of the unmagnetized component I_λ^{scat} (km s^{-1}, relative to the same umbral reference point); the Doppler width of the magnetic component ($\Delta\lambda_D$, in mÅ); the temperature inferred from the source function (T_{B_ν}, in K); the ratio of the linear term to the constant term in the source function (B_1/B_0), with dependencies on filling factor and viewing angle removed; and the line-to-continuum opacity ratio (η_0). For this analysis, the plots cut across the light bridges at their approximate midpoints, and across neighboring umbral regions, as indicated in Figure 1. For guidance, lines indicate the positions of the local umbra (*dotted*) and the bridge (*dashed*) for this slice, according to continuum intensity. This may or may not be the same position as might be defined by, for example, field strength or Doppler width.

4.2.1. *Magnetic Parameters*

The results are systematic for the most part. The continuum intensity is, of course, greater in the bridge than in the umbra, although this difference is less in some bridges, as illustrated with Bridge 10. This is not surprising since the intrusion in Bridge 10 stays at the same intensity level as the transition zone, while Bridge 8 has truly penumbral brightness material. The gradient in the normalized intensity I_c/I_c(qs) from umbra to bridge, of order 0.2 Mm^{-1}, is little different from the normal umbral/penumbral boundary. This is seen by the fact that the width of the transition zone does not change appreciably in most bridge ROIs (see Fig. 1) relative to the normal ROIs.

The magnetic field strength in the bridges is lower than in the umbra, usually by at least 500 G. The two extreme cases are shown in Figure 3, with 300 G in Bridge 10 to over 1200 G in Bridge 8. There were always sections of the bridges that showed gradients in the magnetic field strength of 500 G Mm^{-1} and in some cases a factor of 2 larger (Bridges 1b, 6b, 7b, and 8). These values are lower than a previous study, which observed a gradient of 2000 G Mm^{-1} in the infrared (Rüedi et al. 1995b). The *average* gradient in the magnetic field strength from the umbra to the bridge center through the transition zone was of order 250 G Mm^{-1}, however, and is not significantly different from the normal bridge/penumbra transition zones.

The nonmagnetic fraction α' increases within the bridge relative to nearby umbrae. In Figure 3 the two examples again show the extremes, an increase of 0.1 in Bridge 10, and an increase by over 0.4 in Bridge 8. On the whole, the bridges showed gradients of α' of order 0.2 Mm^{-1}, which was always larger by $\approx$0.1 Mm^{-1} in the bridge ROIs than in the same umbra-to-penumbra transition in normal ROIs.

The deviation of the magnetic field vector from local vertical, $\Delta\gamma$, is larger in the bridge regions compared to the umbra, usually by at least 10°. That is, the fields in the bridges are more horizontal than umbral fields, as shown in Figure 3 for Bridges 8 and 10. The maximum inclination is usually not at the bridge midpoint in these slices. Rather, in all but two bridges, it is offset by 0.5–1 Mm toward a neighboring umbra. Rüedi et al. (1995b) inferred steep gradients in the inclination angle (of order 15° Mm^{-1}) in the umbral/bridge boundary of a broad light bridge. While there are places in almost all bridges studied here where the gradient of the inclination vector between umbra and bridge reaches 20°–30° Mm^{-1}, the average is of order 10° Mm^{-1} in the

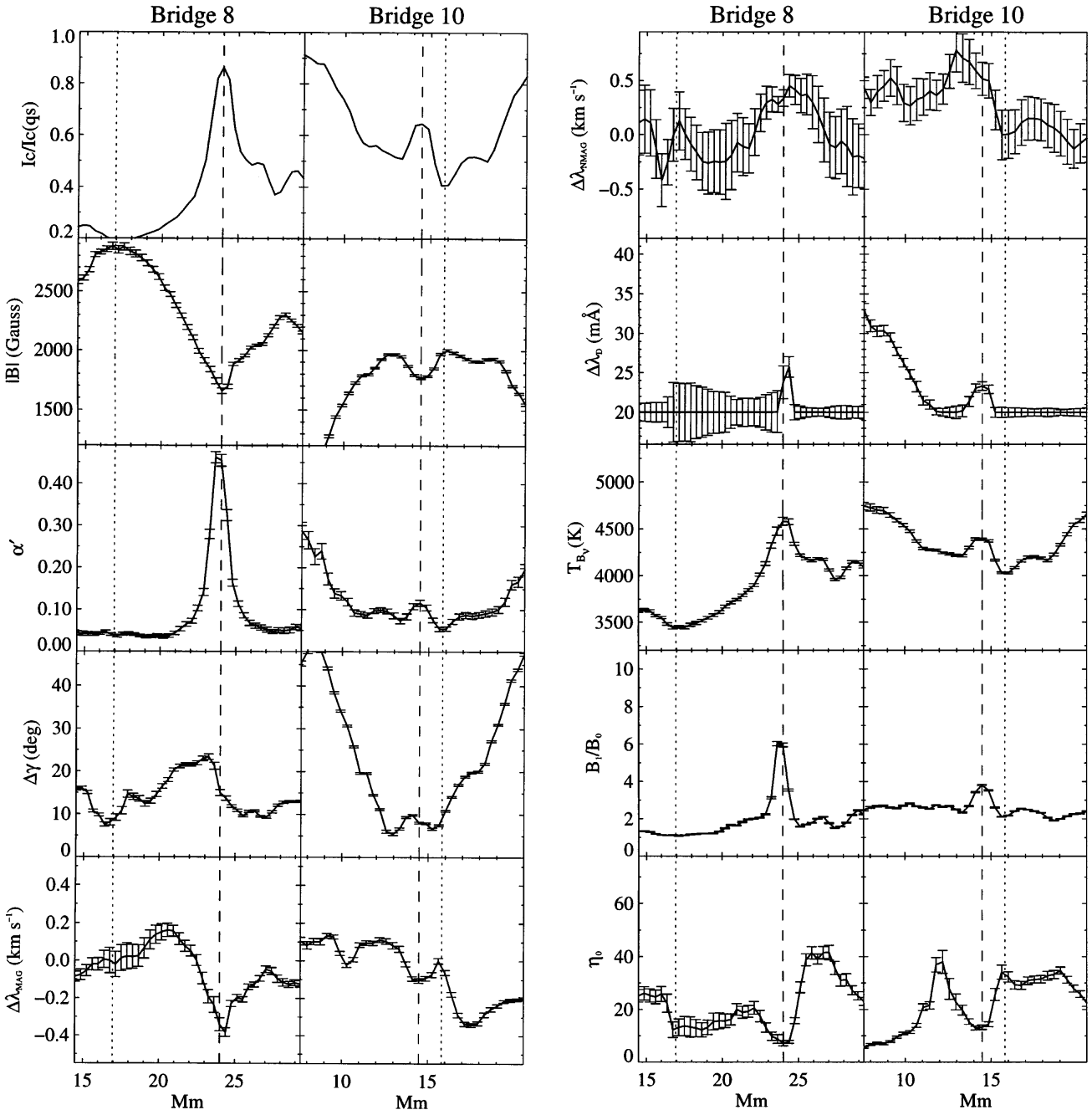

FIG. 3.—Data for a spectrograph slit–like cut across Bridges 8 and 10 and their host sunspots. Vertically we plot the continuum intensity, magnetic field strength, nonmagnetic filling fraction, angular departure from vertical, Doppler shift of the magnetic component, Doppler shift of the nonmagnetic component, Doppler width, temperature derived from the source function, ratio of linear to constant terms in the source function, and last, the line opacity fraction. Vertical lines indicate the approximate midpoints of the bridge (*dashed*) and local umbra (*dotted*) for this slice; velocities are plotted relative to the umbral point. The positional coordinate (Mm) for both Bridges is indicated for comparison with Fig. 1. The formal errors from the inversion are plotted for each parameter except the continuum intensity.

bridge ROI transition zones. This is 2°–5° Mm^{-1} greater than the gradient of $\Delta\gamma$ between umbra and penumbra in the normal ROIs.

It is impossible to appreciate fully the magnetic field azimuthal angle, ϕ, with a slice across the sunspot. In Figure 4 we show the horizontal component of the magnetic field, with the continuum-intensity contours as defined in § 2 and as shown in Figure 1. The examples of Bridges 8 and 10 summarize the situation for all 15 bridge observations. The azimuthal angle in and around the light bridge defines two azimuth centers, each centered on the nearby umbra. The center of the bridge can thus be identified as where the azimuthal angle of the magnetic field is almost parallel to the long axis of the bridge. In Bridge 8, this effect is strong enough to resemble an X-type neutral point. In Bridge 10, the effects is much weaker, although the horizontal fields bunch together and have a more $\hat{y}$ orientation in the vicinity of the bridge than in the rest of Figure 4 [e.g., in the $(x, y) = (15\text{ Mm}, 17\text{ Mm})$ vicinity]. To some extent, this alignment of the azimuth with the bridge, and the divergence of the azimuths along the bridge axis, is observed in all bridges. It is strongest in Bridges 1a, 1b, 7a, 7b, 8, 9, and

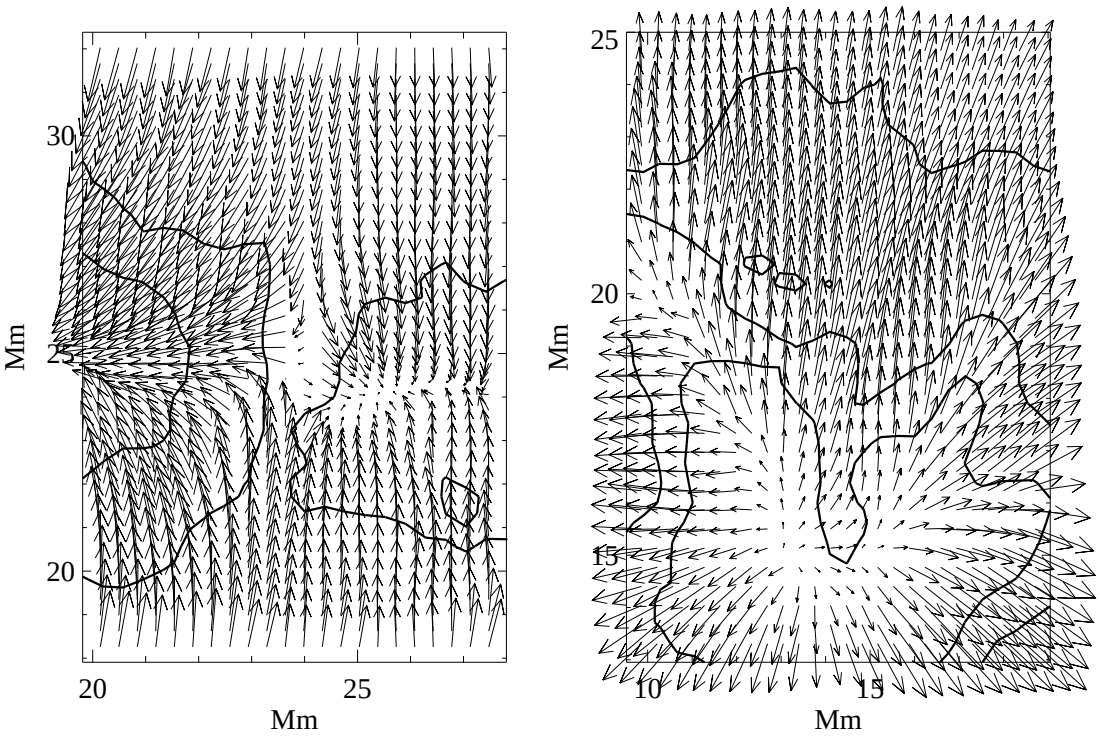

FIG. 4.—Horizontal field component in and around Bridges 8 (*left*) and 10 (*right*). Contoured continuum intensity has identical contour levels to Fig. 1. Maximum vector shown is 1500 G (Bridge 8) and 1200 G (Bridge 10). Scale in megameters for these subimages is shown for comparison with Fig. 1.

11b, weaker in Bridges 2, 4, 5, 6b, 10, and 11b, and weakest in Bridges 3, 6a, and 11a.

4.2.2. *Thermodynamic Parameters*

Shifts of the line center position of the magnetic component $I_\lambda^{\rm mag}$ relative to the umbral line center position ($\Delta\lambda_0^{\rm mag}$) indicate the relative line-of-sight flows in the magnetized plasma at the height of formation of the two spectral lines. Since these sunspots were all $\ll 30°$ of disk center, it represents the vertical flows to a fair degree. In Figure 3, both Bridges 8 and 10 show 0.3 and 0.1 km s^{-1} blueshifts respectively, relative to the umbra. This is fairly representative. In similar slices, nine of the bridges show blueshifted, or upflowing, material (1a, 3, 6b, 7a, 7b, 8, 9, 10, 11b) relative to the umbra with speeds ranging from 0.3 to 0.4 km s^{-1}. Five bridges show redshifted material (1b, 2, 4, 6a, and 11a) at similar speeds, and Bridge 5 shows little Doppler shift. The shear in the flow, as measured in the gradient of this relative Doppler shift, averages 0.1 km s^{-1} Mm^{-1} between umbra and bridge, although it can reach twice that at distinct locations in each bridge ROI. This is not significantly different from the average and the range of shear in the flows in normal ROIs.

The Doppler shift $\Delta\lambda_0^{\rm nmag}$ of the scattered light component $I_\lambda^{\rm scat}$ is also plotted relative to the nearby umbra in Figure 3. For Bridges 8 and 10 there are apparent downflows of almost 0.5 km s^{-1}, although it is also readily apparent that the errors in this parameter are significantly larger than those in $\Delta\lambda_0^{\rm mag}$. It must also be cautioned that the line position of the nonmagnetic fraction of a line profile *in a sunspot umbra* is not a well-defined quantity. Hence, while fully two-thirds of the observations of the light bridges (Bridges 1a, 1b, 2, 3, 4, 6a, 6b, 8, 9, 10, 11a, and 11b) have redshifts relative to $I_\lambda^{\rm scat}$(umbrae) ranging from 0.1 to 1.0 km s^{-1}, it is best to compare this parameter to a different fiducial, as discussed below.

The bridges systematically show a $\Delta\lambda_{\rm D}$ value significantly above the inversion's 20 mÅ lower limit. Only Bridges 5, 6a, and 6b fail to show this increase above the umbral values. On the other hand, in at least four bridges, the increase is of order 10 mÅ in these slices. On average, the gradient in the Doppler width is less than 10 mÅ Mm^{-1} in both bridge and normal ROIs, with little difference between the two.

The temperature derived from the source function is always higher in the bridge regions than in the umbrae. This is somewhat expected given the increased continuum intensity in the bridges, although whether it is a truly higher temperature or simply sampling the temperature at a higher, hotter physical layer is undetermined here.

We see in Figure 3 that the umbral values for the ratio B_1/B_0 are close to 2, as discussed above for regions in radiative equilibrium. In the light bridges, the B_1/B_0 is at least a factor of 2 larger, except in Bridges 5, 6a, 11a, and 11b. The gradient of this parameter through the transition zone generally agrees between bridge and nonbridge regions, averaging 1–2 Mm^{-1}. This is a clear signal that the light bridges have a significant departure from radiative equilibrium.

Every bridge except Bridge 6a shows a decrease in η_0 in the bridges compared to the umbrae. The bridge values generally agree with umbral and penumbral values given in Lites & Skumanich (1990) and Skumanich et al. (1994). They also agree with nonbridge penumbral regions of the host sunspots with similar field strengths. The gradients in η_0 are <20 Mm^{-1} in both the bridge and nonbridge ROIs. This relative reduction of η_0 is also indicative, then, of increased heating in the bridges relative to umbral regions.

A summary for the bridge/umbra comparison results is given in Table 3. However, instead of a slice through the

TABLE 3A

LIGHT BRIDGE VERSUS NEARBY UMBRA

Bridge Number	I_c(U) [I_c/I_c(qs)]	I_c(B) [I_c/I_c(qs)]	B (U) (G)	B (B) (G)	α'(U)	α'(B)	$\Delta\gamma$(U) (degrees)	$\Delta\gamma$(B) (degrees)	$\lvert J_z\rvert$(U) (mA m^{-2})	$\lvert J_z\rvert$(B) (mA m^{-2})
1a	0.28	0.76	2607	1586	0.03	0.25	14	23	7.9	15.7
1b	0.38	0.80	2450	1644	0.04	0.34	10	31	7.0	27.1
2	0.40	0.80	2236	1624	0.10	0.33	8	38	6.8	8.7
3	0.34	0.73	2367	1703	0.05	0.20	11	24	5.8	7.9
4	0.40	0.72	2145	1573	0.07	0.19	10	26	7.4	9.2
5	0.29	0.52	2354	1837	0.02	0.05	13	13	6.6	5.7
6a	0.19	0.43	2566	2378	0.03	0.06	18	34	6.0	8.2
6b	0.25	0.57	2443	2056	0.03	0.14	20	30	6.5	19.5
7a	0.38	0.79	2031	1510	0.07	0.19	13	18	6.6	13.4
7b	0.45	0.85	1844	1436	0.08	0.32	13	9	9.2	35.0
8	0.17	0.71	2936	1794	0.04	0.33	10	20	7.1	47.5
9	0.21	0.85	2841	1350	0.04	0.27	8	19	7.1	12.5
10	0.45	0.61	2097	1704	0.06	0.11	8	16	7.0	6.5
11a	0.40	0.59	2075	1878	0.05	0.08	13	13	8.7	18.3
11b.....	0.36	0.66	2159	1865	0.04	0.10	14	28	13.9	25.6

TABLE 3B

Bridge Number	$\Delta\lambda_{mag}$(B − U) (km s^{-1})	$\Delta\lambda_{nmag}$(B − U) (km s^{-1})	$\Delta\lambda_D$(B) (mÅ)	ΔT_{Bv}(B − U) (K)	B_1/B_0(U)	B_1/B_0 (B)	η_0(U)	η_0(B)
1a	0.03	−0.05	27.4	784	1.8	4.2	30.7	9.4
1b	−0.04[a]	0.05	24.8	715	1.5	3.3	29.2[c]	6.5
2	0.08	−0.27	25.7	726	2.4	5.6	36.1	11.0
3	−0.02	0.20	25.8	532	2.4	4.7	29.4	10.6
4	0.07	0.13	28.9	473	2.6	4.3	48.1	9.4
5	0.17	0.17[b]	20.1	380	1.6	3.1	41.2	33.8
6a	−0.10	0.32[b]	20.0	850	1.2	2.2	24.6	25.5
6b	−0.26	0.24[b]	20.5	783	1.4	3.7	24.5	17.4
7a	−0.15	−0.27	26.6	538	1.6	4.3	28.1	10.0
7b	−0.10	0.11	26.6	597	2.5	4.8	30.6	7.2
8	−0.24[a]	0.48	20.7	1064	1.0	5.6	11.6	10.4
9	−0.13[a]	0.02	29.8	1080	1.2	5.2	13.9	6.1
10	−0.35	0.12	23.7	239	2.2	3.1	36.2	16.0
11a	0.17	0.01	21.8	173	1.9	2.8	41.9	14.8
11b.....	−0.02	0.18[b]	20.4	270	1.7	2.9	29.3	18.4

NOTE.—Errors are as follows: B: ≤2%; α': ≤0.02; $\Delta\gamma$: ≤2°; J_z: $\sigma_{J_z} \approx 10$ mA m^{-2}; $\Delta\lambda_{mag}$: ≤0.04 km s^{-1}; $\Delta\lambda_{nmag}$: ≤0.2 km s^{-1}; $\Delta\lambda_D$: ≤2 mÅ; ΔT_{Bv}: ≤ 100 K; B_1/B_0: ≤0.01; η_0: ≤5. For $\Delta\lambda_{mag}$(B − U), $\Delta\lambda_{nmag}$(B − U) <0 correspond to blueshifts in the bridge relative to the umbral reference.

[a] Error: ≤0.08 km s^{-1}.

[b] Error: ≤0.5 km s^{-1}.

[c] Error: 13.2.

data, we averaged over a 3 × 3 pixel region in the approximate geometric center of the bridge and similarly over a 3 × 3 pixel region centered on the darkest umbral area. Therefore, the areas used may not correspond exactly to those in the slices in Figure 3, and the values entered in Table 3 are an average, instead of a single value. A bridge separates two umbral regions that are unlikely to be identical; we used results for the darker umbra for this comparison. The table reflects what is shown in Figure 3 and the above discussion. There are obvious trends such as increased brightness and decreased magnetic field strength in the light bridges. The nonmagnetic fraction is higher in the bridges, and the fields are generally more horizontal. The Doppler shift of the magnetized plasma is more likely to be blueshifted than not, relative to the mean umbral position. The Doppler shift of the nonmagnetized plasma is referenced here to the mean umbral λ_0^{mag}. This parameter now shows a similar tendency, with two-thirds of the bridges showing blueshift, although the errors are higher for this parameter (as evident from Fig. 3). Since the temperatures derived from the source function are not the result of sophisticated modeling efforts, we list only the temperature difference between the umbra and the bridge. It is above 500 K for the majority of the bridges. The Doppler width of the fitted magnetic component shows a substantial range, however it stays below 30 mÅ, i.e., under the values found for penumbral regions and for quiet sun (Skumanich et al. 1994). The difference $T_{\lambda_D} - T_{B_v}$ implies an increased ξ of order 1 km s^{-1} for most bridges relative to their umbrae. The ratio of the slope to the constant term in the source function, B_1/B_0, is usually around 2 in the umbrae but rises significantly above that in the bridge regions. The line strength η_0 is lower in the bridges than the umbra, except for Bridge 6. These latter two results also generally agree with the results for penumbrae in Skumanich et al. (1994).

4.3. *Light Bridges versus Undisturbed Areas*

4.3.1. *Magnetic Parameters*

In Figure 5 we present scatter plots of the same parameters as analyzed above, but instead of a slice across the light bridges, we compare the parameter in question over the entire ROI for bridge versus nonbridge umbral *and penumbral* regions. These ROIs contain umbral-, transition zone–, and penumbral-brightness points and cover a fairly

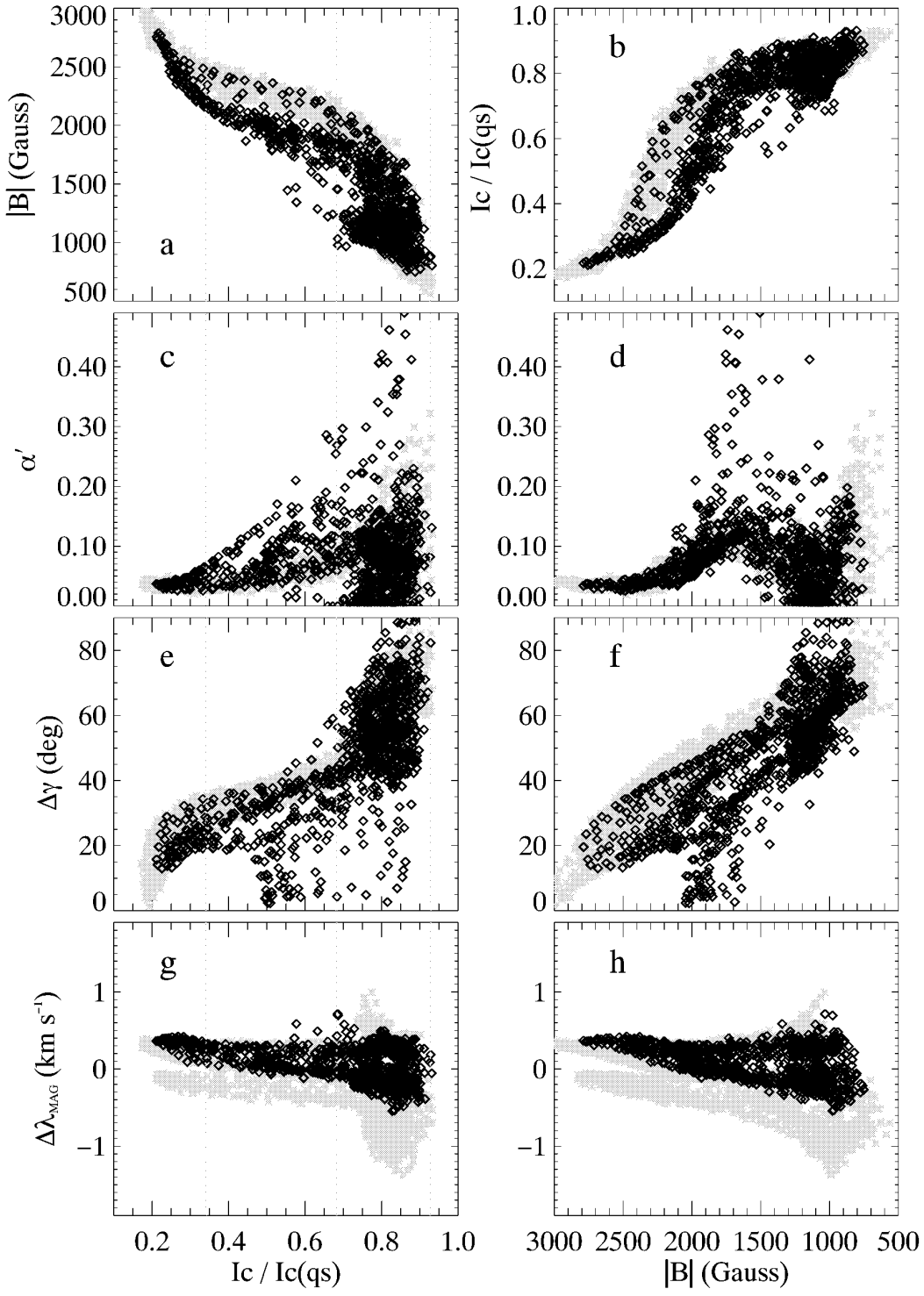

FIG. 5.—Scatter plots of the magnetic and thermodynamic parameters as a function of continuum intensity (*left-hand column*) and field strength (*right-hand column*) for Bridge 8. Points in undisturbed ROIs are gray asterisks; bridge ROI points are black diamonds. The boundary-defining isophotes for umbral cores, transition zone, and penumbra are indicated by dashed vertical lines in the I_c plots. (*a*) Field strength B vs. continuum intensity I_c; (*b*) I_c vs. B; (*c*, *d*) nonmagnetic fraction α' vs. I_c, B ; (*e*, *f*) deviation of the inclination angle from the local vertical $\Delta\gamma$ vs. I_c, B; (*g*, *h*) Doppler shift of the magnetic component relative to the mean umbra $\Delta\lambda_0^{\rm mag}$ vs. I_c, B; (*i*, *j*) Doppler width of the magnetic component $\Delta\lambda_{\rm D}$ vs. I_c, B; (*k*, *l*) temperature derived from the source function T_{B_ν} vs. I_c, B; (*m*, *n*) ratio of the constant to linear source function terms B_1/B_0 vs. I_c, B; (*o*, *p*) line strength parameter η_0 vs. I_c, B.

large area. Hence, even more so than in the previous analysis, using the entire ROIs does not a priori define the light bridge boundaries. Rather, we are comparing what is different about material *in* and *around* a light bridge compared to nonbridge regions. This analysis allows us to examine to what extent the existence of a bridge influences the structure and thermodynamics beyond the immediate umbral intrusion.

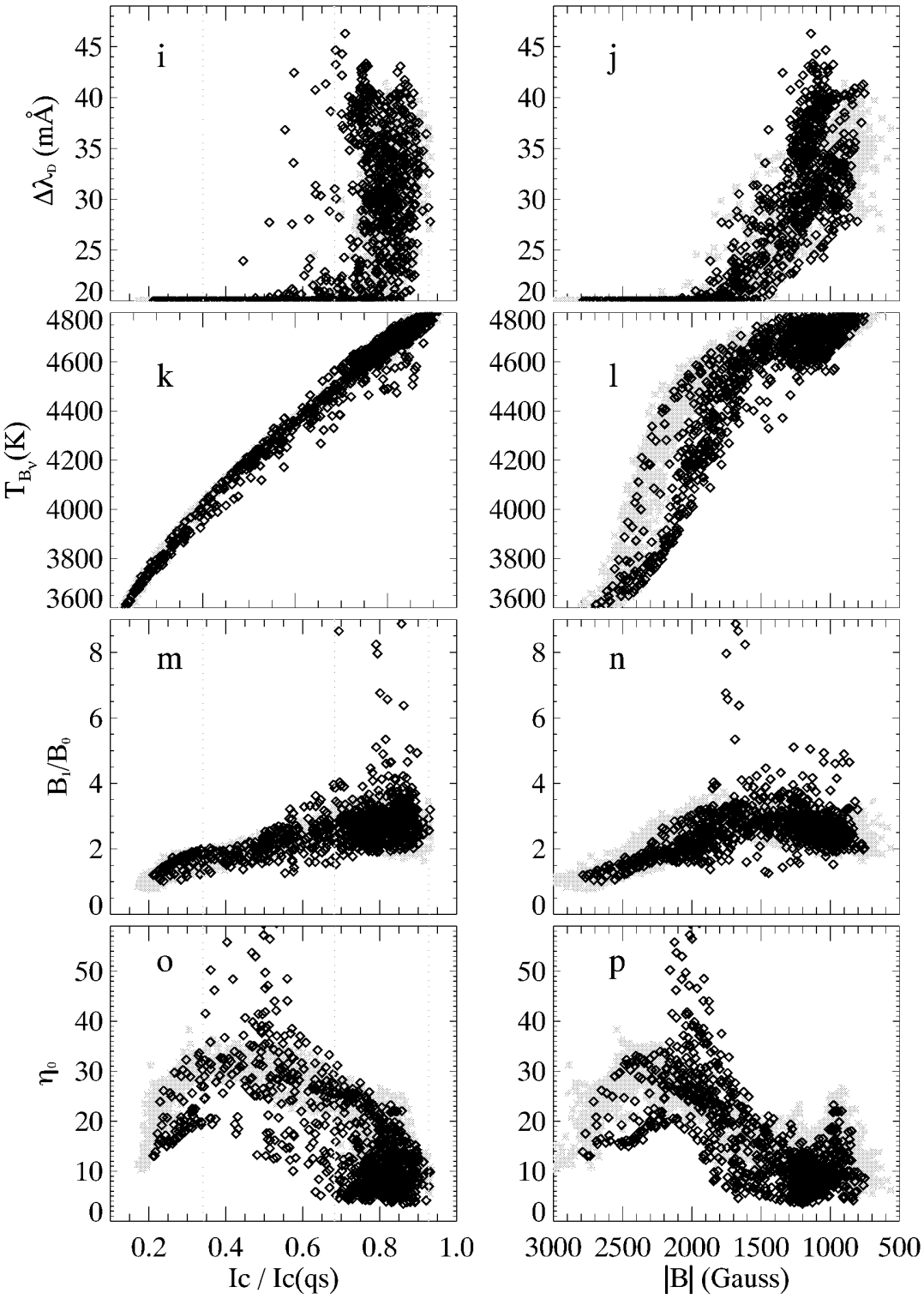

FIG. 5—*Continued*

The magnetic field strength in most bridge ROIs is similar to normal regions, a narrow function with respect to continuum intensity levels with a large spread in brighter areas and a rise in strength with decreasing intensity which is almost linear. The plots of $|\boldsymbol{B}|$ versus I_c (the example of Bridge 8 is shown in Fig. 5*a*) are qualitatively similar to those in previous studies (see, e.g., Lites et al. 1993; Stanchfield, Thomas, & Lites 1997), even including the small upturn away from linearity at the darkest portions of some umbrae. We also plot the reverse, I_c versus $|\boldsymbol{B}|$ (Fig. 5*b*) for comparison with the plots below and following Skumanich et al. (1994). Upon closer inspection, for all bridges except 6a, the points in the bridge ROIs take a different functional form than the normal ROIs. In Figures 5*a* and 5*b*, the majority of the bridge points have a lower field strength than the nonbridge points in the umbra and

transition zone, and the upturn from linearity is sharper in the bridge ROI. Between the bridge and nonbridge points of penumbral brightness, however, there is no significant difference in the $|\boldsymbol{B}|$ versus I_c relation. For other bridges, again the functional form of the relation is different for the bridges and normal areas, but the overall decrease in field strength seen in Bridge 8 is not general. The $|\boldsymbol{B}|$ versus I_c function in undisturbed areas is very consistent from spot to spot, whereas the functional form for this relation in light bridges differs spot to spot.

The nonmagnetic fraction α' is also a fairly tight function of I_c in the umbra and transition zone for normal ROIs (e.g., for Bridge 8; Fig. 5*c*). As expected, it shows a large range in the penumbra. As a function of magnetic field strength (Fig. 5*d*), the nonmagnetic fraction is again tight in strong-field areas, and varied in low-field areas, for the normal ROI. From these two plots, however, it is obvious that there is a much larger spread in the bridge toward higher α' values in the transition zone and penumbra, with a similar spread to higher α' values in areas with 1000–2000 G fields. This effect is strong in all bridges except 6a, 10, and 11a.

The inclination of the magnetic field with respect to the local vertical line is *significantly* different between light bridge and undisturbed penumbral regions. Figures 5*e* and 5*f* show this distinctly for Bridge 8, again as a function either of continuum intensity or field strength. In normal regions, there is an expected multivalue function at higher intensities and lower field strength, corresponding to the range of field inclinations in the outer penumbra. As the brightness decreases toward the umbra, the fields become more vertical, and the range is narrowly defined in the ROIs of undisturbed parts of the sunspot (a similar relation was found in Stanchfield et al. 1997). Systematically, however, the fields in the bridge area are closer to vertical than the nonbridge penumbrae. This effect is strongest in the transition zone and for field strengths 1500–2000 G in Bridge 8; in the other bridges, the bridge fields are always more vertical than normal areas, although the effect may be strongest at higher or lower intensities and/or field strengths. Only Bridge 6a is an exception, showing little difference between normal and bridge areas. The more vertically oriented fields in bridges relative to nonbridge penumbrae contrasts with the finding that the bridges had more inclined fields in comparison with their neighboring umbra.

4.3.2. *Thermodynamic Parameters*

Doppler shifts in sunspots are always tricky to intercompare owing to the effects of the Evershed flows in and around the penumbra, as well as systematics including waves and viewing angles. The scatter plots in Figures 5*g* and 5*h* show the Doppler shift of all points in the ROI's relative to the average umbral line center position of $I_\lambda^{\rm mag}$. Negative velocities indicate a blueshift for the given element relative to the umbral reference. At higher intensities and lower field strengths in both bridge and normal ROIs, there is a large range in velocities owing to the Evershed effect, combined with the varying magnetic inclination and viewing angles across the image. In the darker and stronger field parts of the ROI, there is a redshift in the bridge compared the mean umbral position, but little difference between the bridge and the nonbridge points otherwise. Eight bridges (2, 3, 6a, 7a, 7b, 8, 10, and 11b) showed no distinct overall shift in the bridge points relative to the nonbridge points for the full continuum intensity or magnetic field ranges of the sunspots. Bridges 1a, 1b, 5, and 9 have overall blueshifts in the bridge compared to the nonbridge points, and Bridges 4, 6b, and 11a show an overall redshift.

These results were confirmed when the analysis was performed using histograms rather than scatter plots (again separating the bridge from nonbridge ROIs). The Doppler shift distributions for $\Delta\lambda_0^{\rm mag}$ are either blueward of, or showed little shift relative to, the nonbridge ROI distribution. All but three had distributions blueward of the mean umbral line reference. The shifts of the nonmagnetic component had prohibitive uncertainty and scatter to add any information to this analysis. Nonetheless, we conclude that the light bridges predominantly show upflowing, blueshifted material, relative to the mean umbra. They do not, however, show any trend when compared to the nonbridge regions as a whole.

We examine the Doppler widths statistically in Figures 5*i* and 5*j*. In the darkest, strongest field portions of the sunspot, the values fall to 20 mÅ, and in the penumbral regions $\Delta\lambda_{\rm D}$ generally rises to 30–45 mÅ, in agreement with Lites & Skumanich (1990). The $\Delta\lambda_{\rm D}$ versus I_c and $\Delta\lambda_{\rm D}$ versus $\boldsymbol{B}$ are similar in the bridge and undisturbed areas, except that we see a tendency for larger Doppler widths in the transition zone intensity or medium field strength areas for the bridges than the nonbridge ROIs. In the bridges, the upturn from 20 mÅ to penumbral-like values occurs "earlier" than in undisturbed ROIs for 13 of 15 bridges (all except 4 and 6a), i.e., in the transition zone instead of the penumbra, or at medium instead of low field strengths. This implies a temperature and/or microturbulent velocity increase to penumbral values in some parts of the bridge region even though the intensity and magnetic fields are still closer to umbral values.

The comparison of T_{B_ν} versus I_c and T_{B_ν} versus $|\boldsymbol{B}|$ for the bridge and nonbridge ROIs in Bridge 8 are shown in Figures 5*k* and 5*l*. The former is included only for completeness, since it essentially shows how well the observed continuum intensity agrees with the model atmosphere continuum intensity. The agreement here is excellent, which is expected. The latter plot, of T_{B_ν} versus $|\boldsymbol{B}|$, shows a much different distribution for the bridge and nonbridge ROIs, but similar to I_c versus $|\boldsymbol{B}|$ (Fig. 5*b*). In all but the very highest field strengths, the bridge points are cooler by 100–300 K, compared to points in normal regions at the same field strength. This is true in parts of the umbra, the transition zone, and the penumbra. We find similar relations in six of the bridges (1a, 1b, 4, 5, 8, and 9) with weak or inconsistent differences in the other bridges.

The B_1/B_0 versus I_c and versus $|\boldsymbol{B}|$ plots are shown for Bridge 8 in Figures 5*m* and 5*n*. Again, the former carries little information since the source function essentially defines the intensity, and the tight correlation between the source function terms and I_c is expected. As a function of the magnetic strength, however, the bridge and normal ROIs agree at high field strengths, with a fairly narrow range around 2. There is a larger spread in both normal and bridge ROIs between 1000–2000 G. The even greater spread in the bridge's B_1/B_0 range in this example is representative of the case for two-thirds of the bridges (1a, 1b, 2, 4, 5, 7a, 7b, 8, 9, and 11b).

The line strength parameter η_0 is also intimately tied to the fit to the intensity, and one must carefully interpret the plot of η_0 versus I_c (Fig. 5*o*). What is most significant is that in the plot of η_0 versus $|\boldsymbol{B}|$ (Fig. 5*p*), the bridge points

depart from the nonbridge points in the 1500–2500 G range. There is a conspicuously large number of points in the bridge that have larger values of η_0 than the normal points have. After noting this, we can translate this departure to Figure 5*o* and observe that it occurs in the transition zone exclusively. An umbra and/or transition zone departure of the bridge points from the nonbridge points occurs in 12 of 15 bridges (all but Bridges 3, 6a, and 7b). The *higher* values of η_0 in some bridge ROIs relative to undisturbed ROIs indicate a *lower* heating *when compared to regions of similar intensities and field strengths.*

4.4. *Effects of Scattered Light and the True Magnetic Filling Factor*

It must be noted that the observed increases in the nonmagnetic fractions and the decreased intrinsic field strengths are likely *not* from gross effects of scattered light, for the following reasons. First, the inversion procedure simultaneously represents the observed profile with two components, one each representing magnetized and unmagnetized plasma, the latter represented by a scattered light profile. The magnetic parameters and the effective nonmagnetic fraction are fitted independently, which yields the true field strength. This enables us to separate areas which have high field strength and high nonmagnetic fraction (see, e.g., Martínez, Lites, & Skumanich 1997) from those of intrinsically low field strength (see, e.g., Lites et al. 1995) and hence to separate decreases in intrinsic field strength from increases in the nonmagnetic fraction. Second, light bridges are situated between umbrae, and there is no reason to expect large amount of scattered unmagnetized light in these pixels relative to other umbral pixels, other than that due to the bridge itself. The effect of scattered *polarized* light, on the other hand, would be to introduce a polarization signal where there should be none. In this case, the introduced signal would come from the neighboring umbrae, with field strengths generally over 2 kG. To test this, we utilized a recent upgrade of the HAO inversion code that uses two magnetic components in addition to the nonmagnetic component and examined bridges 1a and 6b. We found that the bridge regions still showed a reduced magnetic field strength relative to the umbral regions of at least 500 G and that any strong field component (i.e., more than 2000 G) was limited to a few percent of the total magnetic filling factor. In any case, the presence of scattered polarized light would have the effect of an *overestimation* of the field strength. Hence, we believe that the regions in light bridges do indeed have lower field strengths and smaller magnetic filling fractions (larger α' values) than umbral areas.

We can actually use the observations of α' from Figure 3, Table 3, and three assumptions to determine the *true* magnetic filling factor f. Recall that the nonmagnetic fraction α' includes the true magnetic filling fraction f, the fraction from scattered light α, and the ratio of the nonmagnetic to scattered-light intensities, $I_\lambda^{\rm nmag}/I_\lambda^{\rm scat} \equiv R$. Our three assumptions are as follows: (1) This ratio R is unity, since using any other value would indicate some knowledge of the intrinsic nonmagnetic profile and the structure of the atmosphere a priori, which we do not have; (2) that the true magnetic fraction f is unity in the darkest parts of the umbra; and (3) the scattered light fraction in the bridges is no larger than in the umbrae themselves. Taking Bridge 1a as an example, α' averaged over 9 pixels in the umbra is 0.03 and averaged over 9 pixels in the bridge is 0.25 (see Table 3). If we assume first $f_{\rm umbra} = 1.$, then the scattered light fraction $\alpha = 0.03$. Application of this to the bridge and assuming $R = 1$ gives us $f = 1.0 + [(\alpha - \alpha')/R] = 0.78$. This implies that 22% of the material in the light bridge is nonmagnetic. Thus, *not only* are the fields intrinsically weaker in the light bridges, but they are also sparser. There is a sizable fraction of field-free plasma in the resolution elements. The generality of this statement for the bridges will be discussed later.

4.5. *Electric Currents and Implied Field Disruption*

The simplest magnetic spot structure is that due to a buried dipole, in which case not only is $\nabla \cdot \boldsymbol{B} = 0$ satisfied but also $\nabla \times \boldsymbol{B} = 0$. Such a simple field approximates many sunspots that are round and simple, with fields vertically oriented at the center umbral regions, and fanning away in the penumbral regions (e.g., in Lites et al. 1993). In such sunspots, the large-scale "twist" of the fields is negligible, which indicates a potential or current-free configuration.

Deviations from a potential configuration indicate an increase in stored magnetic energy, such as has been associated with solar flares (Moreton & Severny 1968; Leka et al. 1993; van Driel–Gesztelyi et al. 1994). Specifically, deviations in the transverse fields from a potential configuration produce "twist," i.e., $\nabla \times \boldsymbol{B} = \mu_0 \boldsymbol{J} \neq 0$, or $\nabla_h \times \boldsymbol{B}_h = \boldsymbol{J}_z$ since we can not measure $d\boldsymbol{B}/dz$ with these data. This calculation was performed for all bridges using a four-point differencing scheme (Fan 1991; Leka 1995), specifically using an approximation for the horizontal magnetic flux, i.e., $\nabla_h \times f\boldsymbol{B}_h$, where $f = 1.0 + (\alpha - \alpha'/R)$, where R is assumed unity and α is estimated as per § 4.4.

It is readily apparent that for the most part, the sunspots studied here had simple structures, save for the existence of a light bridge. None of the bridges used in this study were part of δ-spot regions, the spots as a group had little overall "twist" morphologically, and all of the sunspots (except Bridge 11b's sunspot) had average currents below 10 mA m^{-2}, or just above $1\sigma_{J_z}$ (Table 3). In the bridges, the results were more varied. For example, current densities of almost 100 mA m^{-2} (over $10\sigma_{J_z}$) are present in a portion of Bridge 8, while only a few small patches with current density 40 mA m^{-2} ($3\sigma_{J_z}$) are present in the Bridge 9 region. As mentioned in § 4.2.1, there are also steep gradients in the magnetic field strength at the umbral/bridge boundaries. These gradients average 250 G Mm^{-1} but range up to 1000 G Mm^{-1} in some areas, corresponding to current densities of 80 mA m^{-2} in the latter case. Such high current densities are similar to what one finds in δ-spots (see, e.g., Leka 1995; Skumanich & Semel 1996).

Hence, calculating J_z gives a quantitative measure to the disruption of the horizontal magnetic fields (see § 4.2.1). In most cases, the sunspots as a whole have negligible current as do their penumbrae (to our instrumental and seeing-restricted resolution). However, in nine of the 15 bridge regions, the fields deviate significantly from a potential configuration. In some cases, this disruption is of the same order as found in large flare-productive active regions.

J_z alone, however, does not tell you the direction of the twist relative to the field direction, and J_z can be large in regions where the azimuthal angle of the horizontal fields is not well known (i.e., in weak-field regions but also in sunspot umbrae). One can instead employ the force-free parameter α defined for field-aligned currents by

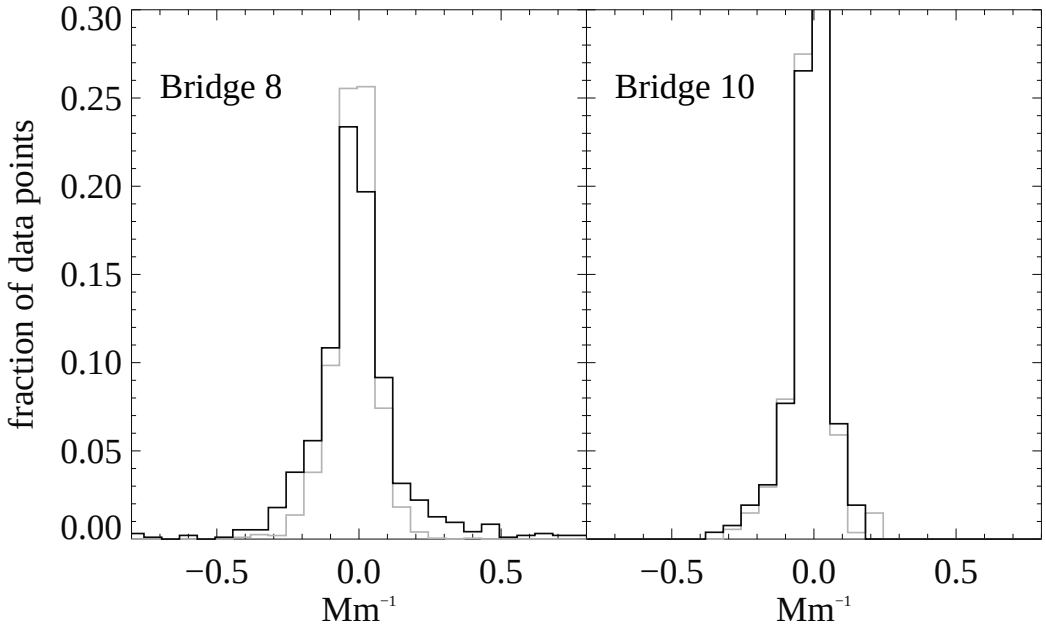

FIG. 6.—Histograms of the value of the force-free parameter α (Mm^{-1}) in the bridge ROI (*black*) and undisturbed ROI (*gray*) for Bridges 8, 10. Each histogram has been normalized to show the fractional distribution.

$\nabla \times \boldsymbol{B} = \alpha \boldsymbol{B}$, or as the ratio[3] $\alpha \equiv J_z/B_z$. This quantity is negative if the field and current are antialigned and is better defined in areas of moderate field strength. We have used this parameter α in two ways. First, one can determine a value of α that characterizes the sunspot as a whole by minimizing the difference between observed transverse magnetic fields and those from constant-α force-free fields computed over a range of α. For the sunspots studied here, this was never above 0.1 Mm^{-1} and was usually around 0.05 Mm^{-1}, i.e., close to the $\alpha = 0$ potential state. In contrast, δ-spot regions routinely show values of this average α above 0.5 Mm^{-1}, a factor of 10 greater (Leka et al. 1996; Skumanich & Semel 1996). Again, the host sunspots are not complicated structures overall.

In general, however, α is *not* constant within a sunspot group, or even within a single sunspot (Pevtsov, Canfield, & Metcalf 1994). For the sunspots studied here, the variation of α values is greater in light bridge regions than not. This is shown in Figure 6, again using Bridges 8 and 10 as examples. The ROIs for the bridges and nonbridge areas are again used here for the comparisons. For all bridges, the distributions of α in both normal and bridge ROIs are centered very close to 0.0. Within the bridge ROIs, however, there is often broader distribution of α (e.g., Bridge 8). This is most significant in Bridges 1b, 2, 4, 6a, 6b, 7b, 8, 9, and 11a. In the other bridges (e.g., Bridge 10), the change is less pronounced.

Calculating $\alpha \equiv J_z/B_z$ indicates once again a disruption of the magnetic fields in the bridge areas, especially when compared to the host sunspot in its entirety. This parameter is useful in addition to simply calculating J_z, since a nonzero value implies a disruption of both the horizontal *and vertical* magnetic field components in the light bridges. Although the degree of difference between bridge and nonbridge areas is small, it is distinctive in those bridges with substantial magnetic field deflections (e.g., Bridge 8). Similarly, it is extremely small or undetectable in those bridges with little disruption, (e.g., Bridge 10).

[3] α is not the scattered light fraction!

4.6. *Summary*

There are distinctions that can be made between bridges and umbrae regardless of morphology. Bridge intensities are higher than in the umbra; this is what historically defines a light bridge. The magnetic fields are weaker and more inclined than umbral fields. The fields' azimuths are aligned to the long axis of the bridge, which effectively defines two separate azimuth centers for each resulting umbra. The nonmagnetic fraction is higher in the bridges than in the umbrae, as are the Doppler widths and their implied microturbulent velocities, while η_0 is lower. The deviation from radiative equilibrium in the bridges, manifest by $B_1/B_0 \gg 2$ in these data, might be a step toward the other extreme, convective equilibrium. This is especially interesting given that it is statistically probable that there are upflows in the bridge area relative to the umbrae.

The comparison of the entire bridge ROI with the undisturbed ROIs confirms some of these trends and brings others to light. The bridges do not generally follow the same relation of $|\boldsymbol{B}|$ to I_c as the undisturbed areas and are generally *less* inclined, especially in areas of reduced field strengths and penumbral-like intensity. The nonmagnetic fraction is higher in the bridge ROIs for a range of intensities and field strengths. The bridge regions show mixed flows relative to the normal nonbridge areas, although they still show predominantly blueshifts relative to the umbra. The bridges can be cooler by a few hundred degrees than nonbridge penumbral areas, and this combined with the smaller η_0 values in the bridges versus nonbridge areas generally confirms the semiempirical model results of Sobotka (1989), although the generality of this will be discussed further below.

It is obvious that these trends vary in magnitude from bridge to bridge. With some parameters, the effects are subtle in some bridges and more pronounced in others. We

now have the general trends; below, we will examine the variations and investigate the causes behind them.

4.7. *The Light Bridge as a Magnetic Canopy*

The evidence presents the following picture: field-free plasma intrudes into the extant magnetic structure from below, as a physical separation is introduced between the umbrae. In stable sunspots with one umbra, the fields fan out from the umbral/penumbral boundary as dictated by $\nabla \cdot \boldsymbol{B} = 0$, forming a magnetic canopy at the penumbral edge. When a light bridge is present, the field lines from these two umbrae will also attempt to fan up and out. They are blocked by the field lines of their neighbor, however, and are forced more vertical than the normally diverging fields from single umbrae. This, in effect, forms a magnetic canopy above a nonmagnetic bridge, similar to that illustrated in Parker (1979c). This canopy structure and the implied magnetic field configuration explains the weaker magnetic field strength in the bridges, similar to the weaker field strengths observed in outer penumbrae (Lites et al. 1993). It also explains the *smaller* observed vertical gradient in the longitudinal field strength, dB_ℓ/dz, *above* a broad light bridge, relative to the gradient observed for the neighboring umbra (Rüedi et al. 1995a). In addition, this canopy or magnetic arcade structure is also consistent with the larger chromospheric line-of-sight field strength found above a light bridge compared to normal penumbra (Rüedi et al. 1995b).

The formation of this canopy is necessarily accompanied by a reconfiguration of the magnetic topology. As discussed in § 4.2.1, the field azimuths begin to reorganize in the narrowest of bridges, which creates a concentration of magnetic field aligned with the bridge axis. As the bridge widens and a separatrix is formed between the now distinct azimuth centers. This is a dramatic topological change. The existence of separatrices has been put forward as a context in which to study magnetic reconnection and flares (see, e.g., van Driel–Gesztelyi et al. 1994). This may be the context in which the reported chromospheric and coronal transient brightenings (§ 1) occur. A detailed model, however, is beyond the scope of the present work.

5. DISCUSSION: VARIETY AMONG LIGHT BRIDGES AND ITS CAUSE

5.1. *Deviations from the Trends*

The generalities of the magnetic field morphology and the thermodynamics in the sunspot light bridges have been summarized above. There is a spread in the degree to which the bridges differ from umbral values for all parameters. To investigate the cause for this variability, let us first clarify which bridges show these effects strongly, which weakly.

In Table 4 we represent the differences between the bridges in terms of how they behave relative to the umbra and undisturbed ROIs. All of the analysis methods described above are used to produce this summary. The limits below or above which a bridge is deemed to have a strong or weak effect is almost arbitrary; nonetheless, these thresholds are listed in Table 4 for each parameter.

It is apparent that some of the bridges, most noticeably those that are predominantly of penumbral intensity (as defined in Fig. 2), are stronger in most categories. Bridges 1a, 1b, 7b, 8, and 9 have large changes in field strength, large nonmagnetic fractions, large vertical currents, and hence have field azimuths that fully and clearly diverge along the bridge toward the two distinct umbrae as Bridge 8 does (Fig. 4). Bridges 5, 7a, 10, and 11a have small drops in the field strength, small nonmagnetic fractions, and show the incipient azimuth alignment similar to the example of Bridge 10 (Fig. 4).

5.2. *Correlations with Bridge Width*

The degree to which bridges were distinct from the umbrae and penumbrae varied noticeably among our examples. This prompted us to search for correlations between the bridge results and their morphological characteristics. Since the host sunspots covered a range of sizes and ages we first investigate correlations with bridge width.

TABLE 4

STRENGTH OF RELATIVE BRIDGE PARAMETERS

Bridge	I_c $\geq$TZ	$\delta\lvert\boldsymbol{B}\rvert$ $\geq$500 G	α' $\geq$0.2	$\delta\Delta\gamma$ $\geq 10°$	$\delta\phi$ Diverged	$\lvert J_z\rvert$ $\geq$20 mA m^{-2}	$\Delta\lambda_{\rm mag} \leq 0$ wrt umbra	$\Delta\lambda_{\rm D}$ $\geq$25 mÅ	$\lvert\Delta T_{Bv}\rvert$[a] $\geq$100 K(P) $\geq$500 K(U)	B_1/B_0 $\geq$3	$\delta\eta_0$ $\geq$15
1a	X	X	X	x	X	x	X	X	x	X	X
1b	X	X	X	X	X	X	X	x	x	X	X
2	x	X	X	X	x		x	X		X	x
3			x	x	x		X	X		X	x
4		X	x	x	x			X	x	X	X
5		x			x		x			x	
6a				X			x		x		
6b		X	x	X	x	x	x		x	X	x
7a	x		x		x		X	x		X	x
7b	X	x	X	x	X	X	X	X		X	X
8	X	X	X	x	X	X	x		X	X	x
9	X	X	X	X	X	x	X	X	X	X	x
10					x	x	x	x		x	x
11a				x		x	x	x			X
11b				X	x	X	x				X

NOTE.—X: strongly follows trends discussed in text, by being strongly above or below threshold given for that parameter in the table; e. g., "$\geq$TZ" refers to whether the bridge is predominantly of penumbral or transition zone brightness. x: weakly or barely makes the threshold. No entry: does not meet the threshold. Whether a bridge meets or does not meet the arbitrary threshold is determined from Tables 2, 3, and the analysis (scatter plots, etc.) discussed in the text. A "δ"X refers to the change between umbra and bridge.

[a] The threshold listed ΔT_{Bv} is a double requirement; that the inferred bridge temperature be 500 K or more hotter than the umbral temperature and 100 K or more cooler than the nonbridge penumbral areas.

TABLE 5

CORRELATION COEFFICIENTS WITH BRIDGE WIDTH

I_c	$\lvert B\rvert$	$\delta\lvert B\rvert$	α'	$\Delta\gamma$	$\delta\Delta\gamma$	$\Delta\lambda_{mag}$	$\Delta\lambda_D$	ΔT_{Bv}	B_1/B_0	η_0
0.41	−0.32	0.54	0.48	0.39	0.60	−0.35	0.33	0.40	0.45	−0.31

NOTE.—δX: the difference between umbral and bridge values were used for the correlation.

The results are presented in Table 5, utilizing the range of bridge widths available.

We searched for correlations not only in the bridge parameters but also in the difference between bridge and umbral parameters in some cases. For example, there is a weak negative correlation between the field strength in the bridge and width, but a stronger positive correlation between the difference between the bridge and umbral field strengths and bridge width. This means that the range of bridge field strengths probably reflects the range in umbral field strengths and that the range itself is only part of the story; the change in field strength from what the stable, mature spot value was (and still is, in the umbra) is more strongly a function of how wide the bridge is.

We find reasonably strong correlation with bridge width of I_c, the nonmagnetic fraction α', the magnitude of the blueshift $\Delta\lambda_{mag}$, the deviation from radiative equilibrium indicated by B_1/B_0, and the temperature increase in the bridges over neighboring umbrae T_{Bv}. There is a similar correlation coefficient for the inclination angle $\Delta\gamma$ and for the field strength decrease $|\boldsymbol{B}|$ with increasing width. The Doppler width $\Delta\lambda_D$ has a smaller correlation with bridge width, as does η_0. However, we find a stronger correlation between the inclination angle difference between the bridge and umbra, $\delta\Delta\gamma$, and similarly with the difference between bridge and umbral field strength $\delta|\boldsymbol{B}|$. These last two, along with the strong presence of a change in the field azimuths (Table 4), signals that the magnetic morphology in sunspots is extremely sensitive to the presence and width of the bridge, possibly more sensitive than the thermodynamic parameters.

These correlations imply one of two things. In one scenario, homogeneous nonmagnetic material occupies a larger fraction of the wider bridges. Hence, an increase in $\Delta\lambda_D$ and decrease in η_0, for example, indicates an increase in the filling fraction of this heated material. On the other hand, changes in these parameters with bridge width could indicate an actual change in the region's thermodynamics, the presence of the heated, nonmagnetic plasma gradually overwhelming any suppressive action the presence of the magnetic atmosphere may have on heating, upflows, etc.

5.3. *Light Bridges: Changes with Time*

Sunspot light bridges can be stable for days, even though they are identified with the breakup of the sunspot itself. In this section, we examine the changes observed in the various magnetic and thermodynamic parameters as these bridges age. Four bridges were observed over more than one day: Bridges 1, 6, 7, and 11. From Tables 2, 3, and 4, and Figure 1, we see that the changes in the bridges as they age are systematic and predictable.

It is obvious that the bridges are wider in the latter of each pair of observations (i.e., Bridges 1b, 6b, 7b, and 11b), either widening the intrusion or completing the umbral split (Fig. 1; Table 2). This is accompanied by an increase in the continuum intensity in the bridges themselves (Table 3). At the same time, the total sunspot area decreases (Fig. 1; Table 2).

The magnetic field strengths in the bridges are smaller in the later observations (Table 3), and the nonmagnetic fractions increase with time (Tables 3 and 4). Accompanying this enhanced "sparseness" in the fields is an increase in the inclination away from vertical (Tables 3 and 4). In addition, as the bridges widen, the horizontal components of the fields become more strongly divergent (Table 4), evolving from a weak alignment of the azimuthal angles along the axis of the bridge (as in Bridge 10; Fig. 4) toward a structure that resembles an X-type neutral point (as in Bridge 8; Fig. 4), the fields along the bridge becoming clearly associated with their closest neighboring umbra. This is reflected in the increased vertical current density for each of the later observations (Table 3).

The Doppler shift becomes more blueshifted in Bridges 1, 6, and 11 (Table 3) as a function of age. In addition, the degree to which the bridge material departs from radiative equilibrium is slightly higher in the later observations for three of the bridges, as is the evidence for increased heating (i.e., a decrease in η_0 (Tables 3 and 4). The temperature differences are not as consistent, however.

These trends are all consistent with the conventional wisdom that the formation of a bridge inside a stable sunspot indicates sunspot decay. This is further supported by the almost full disappearance of sunspot 11's penumbra by 1996 May 14, and of the remnant remaining pores by May 16.[4] Similarly, Bridge 6b's "intrusion" develops to a full umbral split on July 25 (unfortunately μ approached 0.7). In this case, the degree to which the observation of the bridge in Bridge 6a represents "prebridge" observations is a fair explanation for Bridge 6a's weak agreement with the trends discussed above (see Table 4).

On a different note, there have been very few studies in which merging pores have been followed through coalescence to the formation of stable sunspots. Two studies have suggested, however, that the walls or boundaries between the constituent pores are preserved and are in fact the sites where light bridges later develop (Garcia de la Rosa 1987; Zirin & Wang 1990). Unfortunately, these studies have been made only with white-light or longitudinal magnetogram data that carry some morphological information but little information on the physical condition in the most interesting regions.

In this study, one of the light bridges was actually *not* formed during a sunspot's demise but is rather part of the coalescence process. Throughout, we have analyzed Bridge 10 as if it were no different from the others, and it has proved to be a good representative for the other narrower, darker bridges. Bridge 10's sunspot is in fact only 3 days

[4] Bridges 2 and 3 also showed marked decrease in penumbral and umbral area over the subsequent few days, although they rotated off the visible disk before completely disappearing, and unfortunately no additional ASP data were available

old, and flux was still emerging in the active region on March 14. As summarized in Table 4, this light bridge shows weak changes in field strength, Doppler width, etc., even though it is by no means the narrowest or darkest bridge of the 15 observations. This implies that the process of formation and dissolution may be indistinguishable with snapshot data acquisition. This is also a hint that sunspot formation is a physical process which mirrors the sunspot dissolution process. With only Bridge 10 for study, the results are at this time just a hint.

5.4. *Light Bridges: Why?*

The evidence and arguments presented above clearly show that the light bridges are field-free upflowing plasma underneath an arcade of magnetic field lines that are forced to converge locally over the intrusion. This picture does not, however, indicate *why* there are these intrusions into sunspot umbrae in the first place. Thus, we must address the causal relationship question: is there an inherent fragmentation of the magnetic structure that allows the heated plasma to appear between the fragments? Or does the nonmagnetic material penetrate and break up the sunspot?

In Tables 3 and 4 (and in the full analysis that they represent), there is evidence that the magnetic field reorganizes before there is a strong bridge signal in the thermodynamics. The field changes precede the increase in intensity, Doppler width, etc. The field strengths in light bridges show drops of a few hundred gauss even in narrowest, darkest bridges where the increase in the source function gradient and the increased temperature are not strong.

We present the following scenario as the physical cause for the formation of a light bridge. The basic magnetic structure is a bundled flux rope (Parker 1979a, 1984), its "strands" or flux tubes held in close proximity by hydrodynamic drag (Parker 1978, 1979b) and/or twisting and kinking (Piddington 1978; Linton, Longcope, & Fisher 1996; Longcope & Fisher 1996). These strands, when they first emerge, form the pores that coalesce in to the mature sunspot. At some point in the flux system's rise from the subphotosphere into the corona, the tension forces lessen or differential curvature increases (or some other nonequilibrium comes in to play), and the same strands unravel. This overall morphological picture is consistent not only with the observed formation process of sunspots but also with the magnetic reconfiguration that precedes the formation of a full light bridge. It is also consistent with the pore autonomy from coalescence to subsequent sunspot breakup reported by Garcia de la Rosa (1987). In the context of this unraveling, field-free plasma can then penetrate between the flux strands, at that point enhancing the dissolution process of the sunspot as a whole.

The alternative is that an anomalous surge in the surrounding plasma's convection works its way into an otherwise stable structure; i.e., there is some local, preferred change in the plasma $\beta = p_0/8\pi B$. Historically, penetrative convection or some local instability (see Choudhuri 1986) has been viewed as perhaps the reason light bridges are formed. With the results of this study, we conclude that it is rather the end effect.

6. CONCLUSIONS

It has been suspected that the formation of a light bridge in a sunspot begins with an alignment of umbral dots, which are themselves localized sites of convection penetrating through or between magnetic elements in a sunspot (Beckers & Schröter 1969; Muller 1979; Parker 1979c; Lites et al. 1991). While the mechanism behind any alignment and widening process is not yet clear, we can convincingly make the case here for the appearance of convecting, field-free plasma in sunspot light bridges, with the following arguments.

First, the derived magnetic filling factor f, when corrected for scattered light, is substantially lower in light bridges than in the nearby umbra. Often more than 20% of the material in the light bridge is nonmagnetic. The field in the bridge, even beyond the immediate umbral intrusion, is sometimes more filamented even than nonbridge penumbral regions. The strong correlation of the nonmagnetic fraction α' with bridge width supports these findings well; the wider a bridge, the more nonmagnetic material can penetrate, and the smaller the magnetic filling factor.

Second, the thermodynamic parameters indicate heating from below the $\lambda\lambda$6301.5, 6302.5 $\tau = 1$ surface. The decrease in η_0, and the increase in the inferred temperature T_{B_ν} imply a hotter, more ionized atmosphere than is present in the sunspot umbrae. These have similar correlation coefficients with bridge width. The parameter η_0 in the bridges is more consistent with the ranges observed in the unmagnetized quiet Sun around the sunspots than the umbral values (see also Skumanich et al. 1994).

Third, the parameter B_1/B_0 has the strongest correlation with bridge width of the thermodynamic parameters. As discussed above, an increase in this parameter above about 2.0 indicates (in these data) a departure from radiative equilibrium. This may imply that the region is convecting. In addition, since the increase in $\Delta\lambda_D$ is arguably dominated by unresolved velocity fields, the systematically higher Doppler widths and implied microturbulence (ξ) values imply a more turbulent atmosphere in the bridges than in the umbrae, as might be expected if convection was occurring. The increases in the B_1/B_0 and $\Delta\lambda_D$ parameters as bridges widen implies that the material strays farther from radiative equilibrium, instead of there simply being an increase in the nonmagnetic filling factor.

Fourth, most of the bridges showed blueshifted, or upward-moving, material relative to the umbrae. The most straightforward answer for the source of this upflow would be if the bridges contained convecting material that contributed to an overall average blueshifted signal, as the quiet Sun does. There are examples of redshifts in the data, and they may be caused by downflows associated with cooling fronts or other processes affecting hot, unmagnetized plasma in the vicinity of a cool magnetic flux system. For the bridges as a whole, however, convecting plasma is a simple explanation for this and the other three points listed above.

Referring to light bridges, Thomas & Weiss (1991) stated that these "lines of weakness facilitate the eventual breakup of a spot. However, they do not seem to be an essential feature of its structure." This statement may not be consistent with the physical structure of light bridges presented here. The magnetic field lines in light bridges take the form of a magnetic canopy, above the field-free intrusion that appears with the umbra's separation. Above this forming bridge, the normally diverging field lines from the two umbrae are forced to converge above this nonmagnetic intrusion; hence, their more vertical orientation than in the undisturbed penumbra. If a sunspot's magnetic field is an

essential feature of its structure, then the field's rearrangement in the vicinity of a light bridge must also be such an essential feature.

We see evidence for the reorganization of the fields to a canopy-like structure above the field-free intrusion. This is manifest by an alignment of the azimuthal angles along the bridge axis and away from a strictly potential field configuration. Quantitatively, this is seen with stronger vertical currents in the bridges than in the sunspot umbra or in nonbridge penumbra and a wider distribution of the force-free parameter in the wider bridges. The field's reorganization occurs prior to a strong thermodynamical signature. Hence, we argue that the underlying cause for bridge formation is structure inherent in the magnetic flux system. If the sunspot is not monolithic but rather has a structure of a rope or otherwise bundled system of discrete flux tubes, there are already the inherent "lines of weakness" between the individual flux strands, and the flux rope is inherently susceptible to disruption.

We see some correlation of bridge width with continuum intensity, nonmagnetic fraction, field strength decrease, temperature, and the indicators of increased heating and signatures of radiative equilibrium departure. We also observe that the bridges grow wider with maturity. Therefore, the observed correlations are truly *functions of a bridge's age*, and may indicate the sunspot's evolutionary state, and perhaps even how soon it will disappear.

The details of sunspot dissolution must still be studied further. With this presentation of the full vector magnetic field structure and thermodynamic parameters in sunspot light bridges, we now have a clear picture of their structure, their relation to the umbra and to the rest of the undisturbed sunspot. We also present the first steps toward fully understanding how, and possibly why, these bridges form.

The author thanks Bruce Lites, Paul Seagraves, and Randy Meisner for advice on reducing the ASP data; and Barry LaBonte, B. C. Low, Brad Hindman, Phil Judge, Biff Williams, and the referee for very useful chats and suggestions. She is also wishes to heartily thank and gratefully acknowledge Andy Skumanich for invaluable guidance in interpreting the results, minitutorials in radiative transfer, and for a thorough reading of the manuscript. This work and its publication were supported through the Advanced Study Program at NCAR.

REFERENCES

Beckers, J. M., & Schröter, E. H. 1969, Sol. Phys., 384, 403
Bray, R. J., & Loughhead, R. E. 1964, Sunspots (New York: John Wiley & Sons)
Bumba, V., & Hejna, L. 1980, Bull. Astron. Inst. Czechoslovakia, 31, 257
Bumba, V., & Suda, J. 1983, Bull. Astron. Inst. Czechoslovakia, 34, 29
Bumba, V., Suda, J., & Ishkov, V. N. 1981, Bull. Astron. Inst. Czechoslovakia, 32, 286
Bünte, M., Steiner, O., & Solanki, S. K. 1991, in Solar Polarimetry, Proc. of the 11th NSO/SPO Summer Workshop, ed. L. J. November (Sunspot: NSO), 468
Canfield, R. C., et al. 1993, ApJ, 411, 362
Choudhuri, A. R. 1986, ApJ, 302, 809
Collados, M., Martínez Pillet, V., Ruiz Cobo, B., del Toro Iniesta, J. C., & Vázquez, M. 1994, A&A, 291, 622
del Toro Iniesta, J. C., Tarbell, T., & Ruiz Cobo, B. 1994, ApJ, 436, 400
Elmore, D. F., et al. 1992, Proc. SPIE, 1746, 22
Fan, Y. 1991, private communication
Garcia de la Rosa, J. I. 1987, in The Role of Fine-Scale Magnetic Fields on the Structure of the Solar Atmosphere, eds. E.-H. Schröter, M. Vázquez, & A. A. Wyller (Cambridge: Cambridge Univ. Press), 140
Kourganoff, V., with Busbridge, I. W. 1952, Basic Methods in Transfer Problems (London: Oxford Univ. Press)
Labs, D., & Neckel, H. 1968, Z. Astrophys., 69, 1
Leka, K. D. 1995, Ph.D. thesis, University of Hawai'i
Leka, K. D., Canfield, R. C., McClymont, A. N., de La Beaujardière, J.-F., Fan, Y., & Tang, F. 1993, ApJ, 411, 370
Leka, K. D., Canfield, R. C., McClymont, A. N., & van Driel–Gesztelyi, L. 1996, ApJ, 462, 547
Linton, M. G., Longcope, D. W., & Fisher, G. H. 1996, ApJ, 469, 954
Lites, B. W. 1996, Sol. Phys., 163, 223
Lites, B. W., Bida, T. A., Johannesson, A., & Scharmer, G. B. 1991, ApJ, 373, 683
Lites, B. W., Elmore, D. F., Seagraves, P., & Skumanich, A. 1993, ApJ, 418, 928
Lites, B. W., Low, B. C., Martínez Pillet, V., Seagraves, P., Skumanich, A., Frank, Z., Shine, R., & Tsuneta, S. 1995, ApJ, 446, 877
Lites, B. W., & Skumanich, A. 1990, ApJ, 348, 747
Longcope, D. W., & Fisher, G. H. 1996, ApJ, 458, 380
Martínez Pillet, V., Lites, B. W., & Skumanich, A. 1997, ApJ, 474, 810
Metcalf, T. R. 1994, Sol. Phys., 115, 235
Mihalas, D. 1978, Stellar Atmospheres (2d ed.; New York: Freeman)
Moreton, G. E., & Severny, A. B. 1968, Sol. Phys., 3, 282
Muller, R. 1979, Sol. Phys., 61, 297
Ogir, M. B., Parkinenko, L. D., & Stoyanova, M. N. 1985, Sol. Phys., 102, 67
Parker, E. N. 1978, ApJ, 222, 357
———. 1979a, ApJ, 230, 905
———. 1979b, ApJ, 231, 270
———. 1979c, ApJ, 234, 333
———. 1984, ApJ, 283, 343
Pevtsov, A. A., Canfield, R. C., & Metcalf, T. R. 1994, ApJ, 425, L117
Piddington, J. H. 1978, Ap&SS, 55, 401
Rüedi, I., Solanki, S., & Livingston, W. 1995a, A&A, 293, 252
———. 1995b, A&A, 302, 543
Shimizu, T. 1996, private communication
Skumanich, A., & Lites, B. W. 1987, ApJ, 322, 483
———. 1991, in Solar Polarimetry, Proc. of the 11th NSO/SPO Summer Workshop, ed. L. J. November (Sunspot: NSO), 307
Skumanich, A., Grossmann-Doerth, U., & Lites, B. W. 1992, Méthodes de Dètermination des Champs Magnetiques Solaires et Stellaires (Meudon: Observatoire de Paris), 57
Skumanich, A., Lites, B. W., & Martínez Pillet, V. 1994, in Solar Surface Magnetism, ed. R. J. Rutten & C. J. Schrijver (Dordrecht: Kluwer), 99
Skumanich, A., Lites, B. W., Martínez Pillet, V., & Seagraves, P. 1997, ApJS, 110, 357
Skumanich, A., & Semel, M. 1996, Sol. Phys., 164, 291
Sobotka, M. 1989, Sol. Phys., 124, 37
Sobotka, M., Bonet, J. A., & Vázquez, M. 1993, ApJ, 415, 832
———. 1994, ApJ, 426, 404
Solar Geophysical Data. 1992–1996, (Boulder: NOAA)
Stanchfield, D. C. H., Thomas, J., & Lites, B. W. 1997, ApJ, 477, 485
Steinegger, M., Vázquez, M., Bonet, J., & Brandt, P. 1996, ApJ, 461, 478
Thomas, J. J., & Weiss, N. O. 1991, in Sunspots: Theory and Observations, ed. J. J. Thomas & N. O. Weiss (Dordrecht: Kluwer), 3
Title, A., Topka, K., Tarbel, T., Schmidt, W., Balke, C., & Scharmer, B. 1992, ApJ, 393, 782
van Driel–Gesztelyi, L., Hoffman, A., Démoulin, P., Schmieder, B., & Csepura, G. 1994, Sol. Phys., 149, 309
Vázquez, M. 1973, Sol. Phys., 31, 377
Zirin, H., & Wang, H. 1990, Sol. Phys., 125, 45